Nano Research
2023, 16(3): 3781–3803

ISSN 1998-0124 CN 11-5974/O4
https://doi.org/10.1007/s12274-022-5147-z

Review Article

Recent advances in modification strategies of silicon-based lithium-ion batteries

Wenlei Wang, Yu Wang, Lixuan Yuan, Chaolin You, Junwei Wu, Lili Liu, Jilei Ye, Yunling Wu (✉), and Lijun Fu (✉)

State Key Laboratory of Materials-Oriented Chemical Engineering, School of Energy Science and Engineering, Nanjing Tech University, Nanjing 211816, China

Received: 11 July 2022 / **Revised:** 23 September 2022 / **Accepted:** 6 October 2022

ABSTRACT

As potential alternatives to graphite, silicon (Si) and silicon oxides (SiO_x) received a lot of attention as anode materials for lithium-ion batteries owing to their relatively low working potentials, high theoretical specific capacities, and abundant resources. However, the commercialization of Si-based anodes is greatly hindered by their massive volume expansion, low conductivity, unstable solid electrolyte interface (SEI), and low initial Coulombic efficiency (ICE). Continuous endeavors have been devoted to overcoming these challenges to achieve practical usage. This review is centered on the major challenges and latest developments in the modification strategies of Si-based anodes, including structure optimization, surface/interface regulation, novel binders, and innovative design of electrolyte. Finally, outlooks and perspectives of Si-based anodes for future development are presented.

KEYWORDS

lithium-ion batteries, silicon, silicon oxides, modification strategies

1 Introduction

Lithium-ion batteries (LIBs), having the merits of high energy density, high working voltage, long cycle life, and no memory effect, have been effectively applied in various scenarios, such as medical equipment, electric vehicles, mobile phones, and laptops [1–3]. Current state-of-the-art LIBs cannot meet the rapidly growing demand of their daily life and industrial application. In this context, tremendous research has been carried out to pursue higher energy density, faster charge, and improved safety properties [4, 5]. Material innovation and modification are crucial to achieve the goals.

Graphite (Gr) is the most prevailing anode material in commercial lithium-ion batteries, though nongraphitic carbonaceous anode was used in the first generation of Sony lithium-ion batteries. Graphite presents a (de)lithiation plateau close to lithium metal and could offer high and steady voltage. In addition, graphite exhibits excellent cycle stability [6, 7]. However, the theoretical capacity of graphite is 372 $mAh \cdot g^{-1}$, which is not sufficient for high energy and high power applications [8, 9]. And the low redox potential would lead to lithium dendrite formation during fast charging. Various materials were explored as anodes for LIBs, such as Sn, metal oxides, and $Li_4Ti_5O_{12}$ [10–13].

Among the existing anode materials, silicon (Si) exhibits the highest capacity (at ambient temperature, based on $Li_{4.4}Si$, its weight specific capacity is 4,200 $mAh \cdot g^{-1}$) [14, 15], which is ten times as much as conventional commercial graphite. It also possesses merits such as natural abundance (the second most abundant element in earth's crust), non-toxic, eco-friendly, and mild working potential (~ 0.4 V vs. Li^+/Li) [16, 17]. These characteristics make the element a unique and promising anode candidate for LIBs with high energy density. In spite of these advantages, there are also some challenges that seriously restrict the application of Si anodes. Firstly, the severe volume expansion/shrinking of Si (~ 400%) (Fig. 1(a)) during lithiation/de-lithiation leads to the disintegration of silicon powder and electrode cracking (Figs. 1(b) and 1(c)), resulting in fast capacity/voltage fading [18, 19]. Secondly, the large volume fluctuations also cause the exposure of the fresh Si to electrolyte, and continuous decomposition of electrolyte and growth of unstable solid electrolyte interface (SEI) (Fig. 1(d)) [20–23]. Thirdly, the continuous SEI formation results in relatively low Coulombic efficiency (CE), accompanied by a huge amount of Li^+ consumption in irreversible manner during cycling [24–27]. Fourthly, both the intrinsic electron conductivity (10^{-5}–10^{-3} $S \cdot cm^{-1}$) and the ion mobility (10^{-14}–10^{-13} $cm^2 \cdot s^{-1}$) of silicon are poor (Fig. 1(e)) [28–31], giving rise to unsatisfactory rate performance of silicon anodes. Finally, silicon anode materials for LIBs may emit combustible gases produced by electrolyte decomposition, which may cause the decrease of Coulombic efficiency and sometimes fire or explosion (Fig. 1(f)) [32].

On the other hand, silicon oxides (SiO_x, $0 < x \leq 2$), another silicon-based anode, are viewed as attractive alternatives to silicon, on account of their low cost and easy synthesis. Importantly, silicon oxide-based anodes realize a tradeoff between discharge capacity and volume change compared with Si anodes. Silicon oxides can react with Li thermodynamically by a multi-step process to form Li_2O and lithium silicates irreversibly during the first lithiation, showing a relatively small expansion (~ 200%). The generated Li_2O and lithium silicates may act as buffer components

Address correspondence to Yunling Wu, ylwu@njtech.edu.cn; Lijun Fu, l.fu@njtech.edu.cn

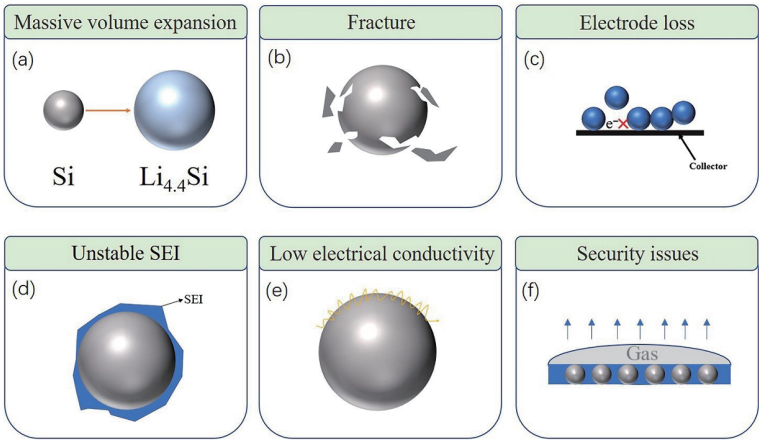

Figure 1 The schematic illustrations of the main problems of silicon-based anodes.

to accommodate volume change on charge/discharge cycling, resulting in the improvement of cycling stability. Nevertheless, the process of silicon oxide anode materials is held back by the low electrical conductivity, low initial Coulombic efficiency (ICE), and serious side reactions with electrolyte.

Tremendous efforts have been made to address these problems [33–35]. The bulk expansion and poor conductivity of Si can be effectively alleviated, and the conductivity can be enhanced, yet it is still quite away from the industrial application. So far, several reviews on Si or SiO_x anodes in lithium batteries have been reported individually [36–38]. However, to the best of our knowledge, a comprehensive investigation on the electrochemical performance optimization methods of Si and SiO_x is lacking. In this contribution, the latest advances on solutions and strategies to increase the electrochemical performance of Si-based lithium-ion batteries are reviewed. We will introduce the modification strategies in detail, including structure optimization, interface regulation, novel binders, and innovative design of electrolyte (including solid-state electrolyte in silicon-based batteries) (Fig. 2). At the end of this article, the perspective of Si-based anodes for practical application is discussed.

2 Modification strategies

2.1 Structure optimization

Nanostructure design is a very efficient strategy to enhance the performance of Si-based anodes for LIBs, because it can alleviate the crushing effect of Si or SiO_x during cycling and maintain the integrate structure, and shortens the ion/electron diffusion path. Generally, the nanostructured Si can be categorized as nanoparticles (zero-dimensional (0D)), nanowires, nanorods and nanotubes (one-dimensional (1D)), nanosheets (two-dimensional (2D)), and nanoframeworks (three-dimensional (3D)) [39–44].

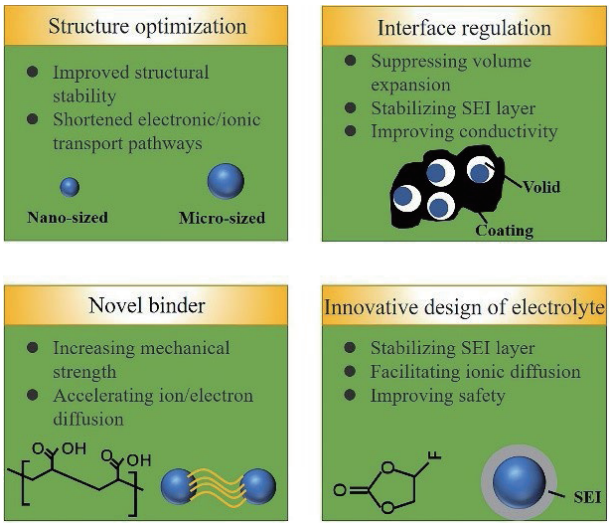

Figure 2 The main modification strategies of Si-based anode in LIBs.

2.1.1 0D nanoparticles

Generally, zero-dimensional nanostructured materials have a high surface area to volume ratio (SA/Vol), leading to less absolute volume change of Si or SiO_x particles in the process of charge and discharge [45, 46]. It was reported that surface cracking and particle fracture did not occur when Si particle size was below 150 nm [47]. For instance, Cho and his coworkers prepared ultra-dispersed Si nanoparticles (n-Si) with different particle sizes (5, 10, and 20 nm) in reverse micelles at high pressure and temperature [48]. When these samples were used as anodes for LIBs, no obvious surface cracking and particle growth after cycling were observed. It could be attributed to the high SA/Vol, and the dislocations could be rapidly drawn to the surface. All of the samples achieved high initial charge capacity and long cycle stability, particularly the 10 nm sized n-Si nanoparticles covered by carbon layers. As for SiO, reducing particle size is also effective to improve its electrochemical performance. Sohn et al. conducted high energy mechanical milling (HEMM) followed by surface etching with NaOH to obtain smaller size m-SiO (NaOH) particles (less than 10 μm in diameter) [49]. The as-prepared m-SiO (NaOH) showed a high initial capacity of ~ 2,400 $mAh{\cdot}g^{-1}$ and long cycle stability with 86.5% capacity retention. The capacity and cyclability were improved with decreased particle size and the removal of oxygen-rich SiO_x on the m-SiO (NaOH) particles surface which would block the Li^+ diffusion (Fig. 3(a)). Nevertheless, the commercial LIBs based on Si-based nanoparticle anodes have encountered a bottleneck. The inherent high specific surface area of Si and SiO_x nanoparticles can lead to serious irreversible side reaction, resulting in the continuous consumption of electrolytes and the repeated generation of SEI layer.

2.1.2 1D nanomaterials

1D nanowires, nanorods, or nanotubes exhibit the advantages similar as 0D nanoparticles, such as suppression of volume expansion and electrode pulverization, and enhancement of lithium/electron diffusion. In addition, the 1D nanomaterials help overcome the aggregation of 0D nanoparticles and reduce the interfacial barrier caused by particle contact for electron transport [50]. For example, Zhou et al. reported a hierarchical Cu-Si nanowire structure with Al_2O_3 coating (denoted as HCS NW) by using a bottom-up strategy involving an annealing process in air followed by a plasma enhanced chemical vapor deposition

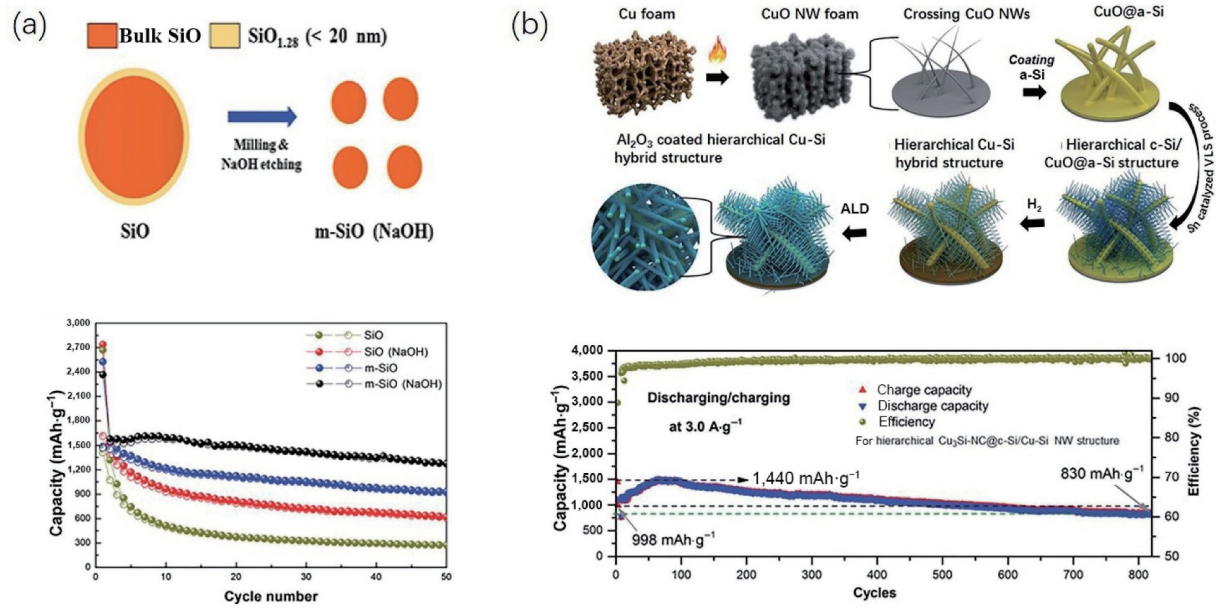

Figure 3 0D silicon-based nanomaterials. (a) Schematic view of the preparation of m-SiO (NaOH) and corresponding cycling performance at 150 mA·g^{-1}. Reproduced with permission from Ref. [49], © The Royal Society of Chemistry 2013. 1D silicon-based nanomaterials. (b) Preparation process of the HCS NW structure and cycling stability of the HCS NW hybrid anodes at 3 A·g^{-1}. Reproduced with permission from Ref. [50], © The Royal Society of Chemistry 2018.

(PECVD), a vapor–liquid–solid (VLS) process with a SiH_4 source, an annealing process in H_2, and finally the atomic layer deposition (ALD) technology (Fig. 3(b)) [50]. Cu-Si alloy conductive matrix afforded numerous electron transfer routes along the axial direction of the nanowires. Meanwhile, the migration barrier for Li^+ diffusion in the radial direction was effectively reduced. Besides, the hierarchical alloying arrangement greatly improved the Si loading (up to 1.3 mg·cm^{-2}) and its electrical conductivity. Such an HCS NW hybrid buffer structure accommodated volume changes on charge/discharge cycling. Therefore, the HCS NW anode delivered a reversible capacity of ~ 830 mAh·g^{-1} at the end of 800 cycles at 3.0 A·g^{-1} with a high capacity retention of 85% (Fig. 3(b)). Mai et al. carried out a novel self-sacrificed of bimodal mesoporous silica (BMS) method to obtain porous core–shell nanowire arrays with SiO_x core and carbon shells (pC-SiO_x NWs) [51]. A large quantity of Fe^{3+} ions from $FeCl_3$ were adsorbed in the pores of BMS and boosted the growth of SiO_x nanowires. Such a structure buffered the volume expansion and maintained a robust SEI layer outside the carbon upon lithiation/delithiation process, resulting in an outstanding cycling stability with reversible discharge specific capacity of 623 mAh·g^{-1} after 150 cycles at 500 mA·g^{-1}. Although 1D Si or SiO_x nanowires can effectively enhance the electrochemical performance of lithium-ion batteries, they have more complex structure and higher manufacturing costs compared with 0D silicon nanoparticles (SiNPs) [52].

2.1.3 2D nanofilms

The contact region between the electrode material and the current collector can be greatly increased by 2D Si-based thin film with a large specific surface area, which is conducive to the rapid ion/electron diffusion in electrodes and battery life extension [53, 54]. For example, Peng et al. deposited patterned Si and ZnO layers in sequence on Cu foil followed by coating carbon as the outer layer via magnetron sputtering to prepare tri-layer composite films (Si/ZnO/C, SZC) with the thickness of ~ 85 nm [40]. The thick electron-conductive carbon shell protected Si layer from electrolyte infiltration and facilitated the formation of robust and stable SEI film. Then, the carbon layer was partially replaced by the Li_2O-Zn layer after the first cycle, accelerating the migration rate of Li^+ and electrons through the interface buffer layer. Moreover, the well-designed Li_2O-Zn layer with supreme elasticity mitigated the volume change of Si active layer, which contributed to sustaining the structural integrity of the anode material. Therefore, the Si/Li_2O-Zn/C composite film delivered a high reversible capacity of 1,536 mAh·g^{-1} after 800 cycles at 1.0 A·g^{-1} and a high-rate discharge capacity of 1,400 mAh·g^{-1} after 6,000 cycles at 10 A·g^{-1} (Fig. 4(a)). In addition, Xu and coworkers prepared dispersible silicene nanosheets for the first time by liquid oxidation and exfoliation of $CaSi_2$ with the oxidant (I_2) in acetonitrile [41]. The $CaSi_2$ could be converted to CaI_2 with high solubility and Si framework by the oxidation reaction in the presence of I_2. Then silicene sheets were exfoliated from bulk Si framework in acetonitrile. The as-prepared ultrathin silicene sheets were few-layer thickness of 3–4 nm but exhibited excellent crystallinity and mechanical property. The chemical stable silicene nanosheets retained 721 mAh·g^{-1} close to its theoretical value at 0.1 A·g^{-1} after 100 cycles (Fig. 4(b)). Zhang et al. synthesized a bilayer nanomembrane consisting of alternating Si-rich SiO_x layer and O-rich SiO_y layer with the chosen oxygen contents by industry-compatible thin film deposition rolled-up technique [55]. The resultant product facilitated Li^+ transport and restrained the volume expansion of silicon oxides. Therefore, a large reversible capacity of ~ 1,300 mAh·g^{-1} at 100 mA·g^{-1} was retained. However, it should be noted that the dense films would generate tensile stress on the Si or SiO_x phase upon lithiation, leading to surface cracking, which in turn influences the performance of the battery.

2.1.4 3D nanoframeworks

The interconnected Si and SiO frameworks ensure adequate contact between electrode and electrolyte, offering highly efficient conductive networks for lithium ions, thus greatly improving electrochemical properties.

Additionally, 3D silicon-based nanoframeworks, especially hollow and porous Si and SiO_x, have attracted growing attention because the hollow and/or porous structure can supply enough room for the expansion of Si/SiO_x without cracking or crushing [56]. Zhi et al. developed interface stabilized siliceneflowers, consisting of numerous interconnected 2D silicene nanoflakes with different spatial orientations resembling the petals of the flower [57]. Such a three-dimensional flower-like structure made the inside space accessible, improving the structural stability and shortening ion/electron diffusion length. As a consequence,

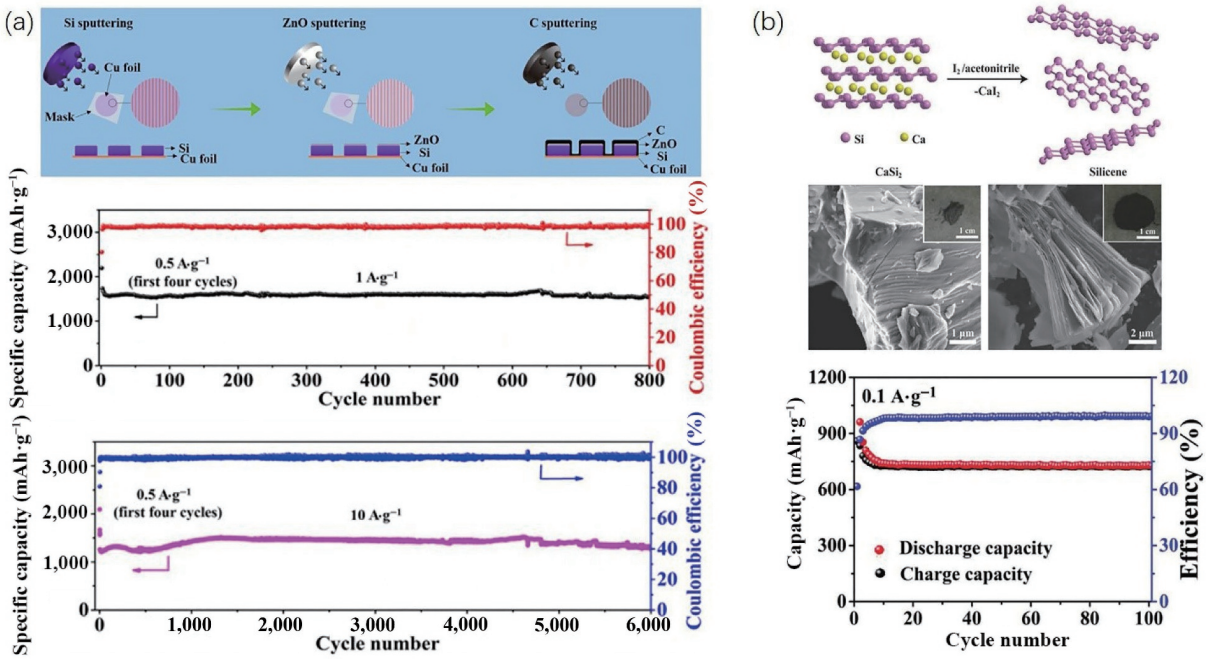

Figure 4 2D silicon-based nanomaterials. (a) Synthesis of the SZC film electrode and its cycling performances at 1.0 and 10.0 A·g^{-1}. Reproduced with permission from Ref. [40], © WILEY-VCH Verlag GmbH & Co. KGaA, Weinheim 2019. (b) Schematic illustration for the synthesis of silicene from $CaSi_2$ via liquid oxidation and exfoliation; scanning electron microscopy (SEM) images of pristine bulk $CaSi_2$ and its cycling performance. Reproduced with permission from Ref. [41], © WILEY-VCH Verlag GmbH & Co. KGaA, Weinheim 2018.

excellent cycling stability was obtained under 2,000 mA·g^{-1} after 600 cycles with a reversible specific capacity of 1,100 mAh·g^{-1} (Fig. 5(a)).

Chen and coworkers innovatively constructed the porous SiO_2 particles by evaporation of crystal water from perlite and then produced porous Si through magnesiothermic reduction reaction [58]. After that, the surface of porous Si core was encapsulated by Ni-incorporated and N-doped carbon nanotube arrays (Ni-NCNTs) and followed by forming Ni_2Si alloy at the interface to fabricate a unique core–shell-structured NCNTs-Ni_2Si@Si. The rich pore structures of porous Si and large void space in NCNTs were beneficial for controlling the volume expansion of Si and enhancing the Li^+ diffusion and offering rich active sites for Si utilization at the same time. Moreover, the Ni_2Si alloy at the heterojunction interface between the Ni-NCNTs and porous Si exhibited good electrical conductivity as well as avoided the detachment of CNTs from the surface of porous Si core effectively in the charge and discharge process. For these reasons, NCNTs-Ni_2Si@Si anode achieved a considerable capacity of 1,547 mAh·g^{-1} and good cycling stability with 85% capacity retention after 100 cycles at 358 mA·g^{-1}. Di et al. synthesized hollow Si spheres by high temperature reduction of carbon-coated SiO_2 with the help of Al powder [59]. The carbon layer played a vital role in regulating the diffusion of reactants and facilitating the mass transfer at the interface and therefore promoting the construction of hollow structure. Such a hollow structure created intimate electrode–electrolyte contact and reduced the volume changes of porous Si during cycling. The as-synthesized silicon hollow structures displayed a stable discharge capacity of 1,774 mAh·g^{-1} after 200 cycles at 1 A·g^{-1} (Fig. 5(b)).

Despite these efforts, progresses in the application of porous silicon electrode are still hindered by its poor conductivity, small volume capacity, low weight energy density, and low tap density. On the other hand, various structural design strategies of porous SiO are implemented to regulate the formation of pores. Sohn et al. obtained d-SiO particles based on the well-known disproportionation reaction of SiO ($2SiO \rightarrow Si + SiO_2$) [60]. Then, nanocrystalline Si was removed by NaOH solution, but SiO_2 matrix was preserved, forming a porous structure of SiO_x (P-SiO_x). Due to the unique structure and fluent Li^+ transport channels, the P-SiO_x manifested a large reversible capacity of ~ 1,240 mAh·g^{-1} over 100 cycles with a Coulombic efficiency close to 100% (Fig. 5(c)). Chen et al. designed a special Si/C/void/SiO_2/C nanostructure via HF selectively etching the SiO_2 layer [61]. This special structure provided excellent electron transport capabilities owing to the high electrical conductivity of the inner and outer carbon walls. Furthermore, the central void offered ample room for Si particles to expand and contract during cycling, maximally avoiding surface cracking and electrode pulverization. As a result, the unique structure exhibited a high first discharge capacity of 1,641 mAh·g^{-1} and an acceptable ICE of 64% at 100 mA·g^{-1} (Fig. 5(d)).

2.1.5 *3D current collectors and binder-free electrodes*

Additionally, 3D current collectors as a potential alternative to planar Cu foil can not only increase the interfacial interaction between Si/SiO_x and current collectors, thereby C-rate performance, but also accommodate the volume expansion. 3D current collectors can be divided into two categories, metal foams [62, 63] and porous carbons [64, 65]. For example, Hamankiewicz et al. prepared a 3D Cu collector with great mechanical stability than planar Cu foil by electrochemical deposition of Cu in water [66]. The 3D current collector with the mass loading of 0.2 mg·cm^{-2} of SiNPs sputtered by radio frequency (RF) magnetron sputtering exhibited good cycling stability of 0.2% capacity fade per cycle and high specific capacity of about 376 mAh·g^{-1} at 0.1 C. Liu et al. reported a carbon foam carbonized from melamine formaldehyde, followed by an anneal process to deposit Ti film and Si film on the carbon foam via electron-beam evaporator [67]. The obtained electrode displayed a long cycling life (up to 1,000 cycles) and excellent capacity retention (average 0.009% decay rate per cycle).

Generally, polymer binders are electrochemical inactive, reducing the overall energy density and increasing the polarization of Si-based electrodes. Thus, the removal of binders to engineer binder-free electrodes is a promising pathway to improve the Si-based anodes electrochemical performance. For example, Zuo et

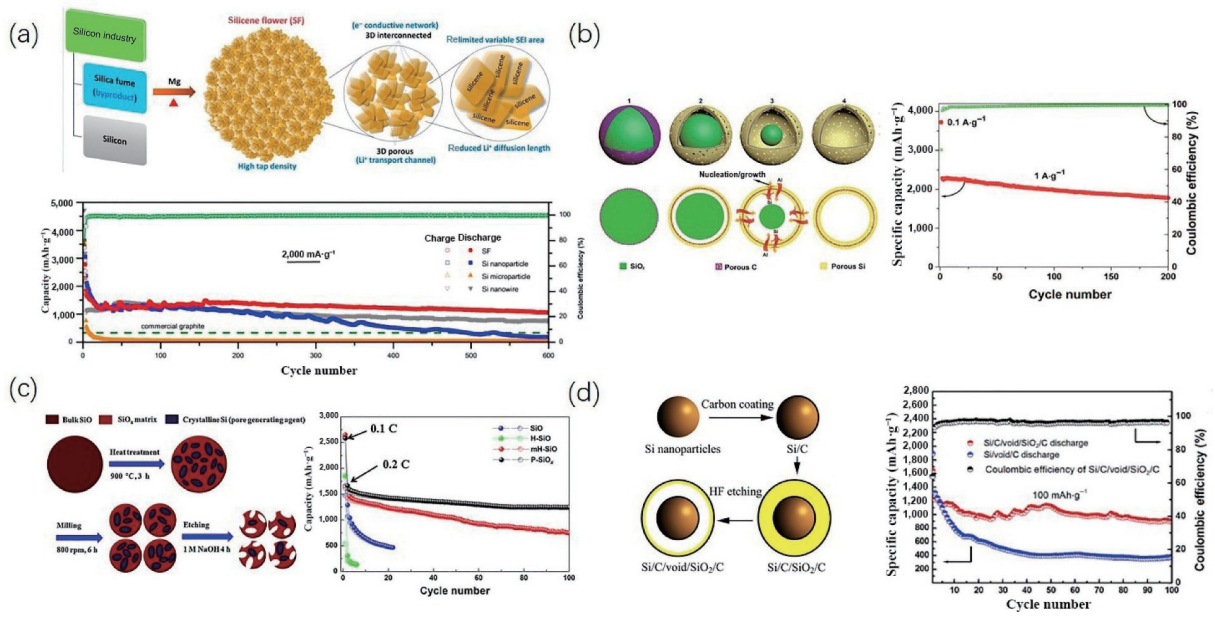

Figure 5 3D silicon-based nanoframeworks. (a) Schematic of the production process of silicene flower (SF) and cycling performance of the SF over 600 cycles at 0.5 C (2,000 mA·g^{-1}). Reproduced with permission from Ref. [57], © American Chemical Society 2017. (b) Schematic illustration of the formation of silicon hollow nanostructures through reduction of silica with Al powder in molten salts and cycling performance of the silicon hollow spheres. Reproduced with permission from Ref. [59], © American Chemical Society 2018. (c) Schematic views of the preparation of porous SiO_x and long cycling performance of different anodes. Reproduced with permission from Ref. [60], © Elsevier Ltd. 2013. (d) Schematic representation of the synthesis procedures of Si/C/void/SiO_2/C nanoparticle and its cycling performance. Reproduced with permission from Ref. [61], © Elsevier B.V. 2018.

al. prepared a binder-free reduced graphene oxide/silicon (RGO/Si) composite by ultrasonic dispersion of the colloid RGO and SiNPs [68]. The colloid RGO could adhere to the SiNPs due to its flexibility, which was crucial to construct the binder-free structure. The layered RGO boosted the Li^+ transport and sustained the integrity of SiNPs, thus improving the cycling and rate performance. Moreover, Si/SiO_x was reduced from SiO by Tan et al. through high energy ball milling, and then coated with nitrogen-doped carbon from polyacrylonitrile as carbon sources via annealing [69]. The nitrogen-doped carbon with high electrical conductivity ensured high Li^+ mobility and structural integrity.

2.2 Surface/interface regulation

Generally, the repeated formation of SEI resulting from the large specific surface area of nanosized Si or SiO_x anode materials often brings about low ICE and poor cycling stability [70]. Moreover, low inherent electronic conductivity of Si-based anode materials restricts their industrial application as well [71, 72]. Therefore, surface and interface modulation are always used in the lithium-ion batteries for the purpose of more effectively achieving targeted electrochemical performance. In recent years, with the expanding understanding of surface and interface enhanced mechanism, reasonable design of surface/interface engineering of Si or SiO_x has been developed to overcome these drawbacks. The surface coating is regarded as an effective way of surface/interface regulation to prevent the direct contact between Si/SiO_x and electrolyte, which inhibits repeated broken and generation processes of SEI. Furthermore, the coated layer provides fast transport pathways for Li^+ and electrons and reduces the mechanical stress caused by the large volume changes [73, 74]. In this section, recent developments in optimizing the surface coating for promoting the electrochemical performance of Si and SiO_x anodes are presented. The introduction of surface/interface regulation is divided into three parts: carbon coating, metals and metal oxides coating, and polymer coating [75–83].

2.2.1 Carbon coating

The main functions of carbon as a coating layer of Si/SiO_x are as follows: (1) The carbon layer improves the electrical conductivity of Si-based anodes remarkably; (2) the carbon-based coatings efficiently prevent electrolyte infiltration into Si/SiO_x particles via interparticle cracks, by building a more stable SEI layer; (3) the carbon shell avoids the agglomeration of Si/SiO_x nanoparticles; and (4) the suitable elastic buffer carbon shell accommodates huge volume changes of Si/SiO_x during lithium intercalation/deintercalation process [70, 78, 80, 84–98]. A novel approach was proposed by Yang and coworkers to synthesize three conductive carbon materials (carbon black (CB), graphene, and carbon) coated micron-sized Si spheres (Si/CB@G@C) via a water-in-oil (W/O) system [75]. The micron-sized graphene sphere in such a hierarchical structure acted as a buffer layer to control the volume changes of SiNPs and enhanced the electrical conductivity to improve stability. The tri-layer carbon shells connected with SiNPs and CB together with graphene effectively prevented the infiltration of electrolyte into Si core. Therefore, the as-prepared Si/CB@G@C hybrids yielded a good rate performance with the capacity of 728 mAh·g^{-1} at 2 A·g^{-1}, which was superior to that of Si@G and pure Si (Fig. 6(a)). Actually, Zhang et al. found that the charge–discharge capacity of the core–shelled silicon-carbon composites decreased with the increase of carbon content, and yet the ICE increased gradually. In addition, the thickness of the soft-packed lithium-ion batteries became thicker during the charge/discharge process under a high silicon content, leading to serious expansion of negative electrodes and the electrochemical performance degradation [99].

The anisotropic expansion of micron-sized silicon anodes simply causes crack initiation and propagation. Aiming to address this problem, Yang et al. constructed an imperfection-tolerant unique carbon capsule cellular (3C) architecture through chemical vapor deposition (CVD) with a CH_4 source followed by precise etching of inner voids with NaOH, consisting of carbon cages interweaved in graphene network (SiMP@C-GN; SiMP = Si microparticle) [100]. With large void space inside, SiMP@C-GN had mechanical strength and ductility, showing a great lifetime over 1,000 cycles with an average Coulombic efficiency over 99.5%. More importantly, no obvious crack and pulverization of particles were observed after cycling (Fig. 6(b)).

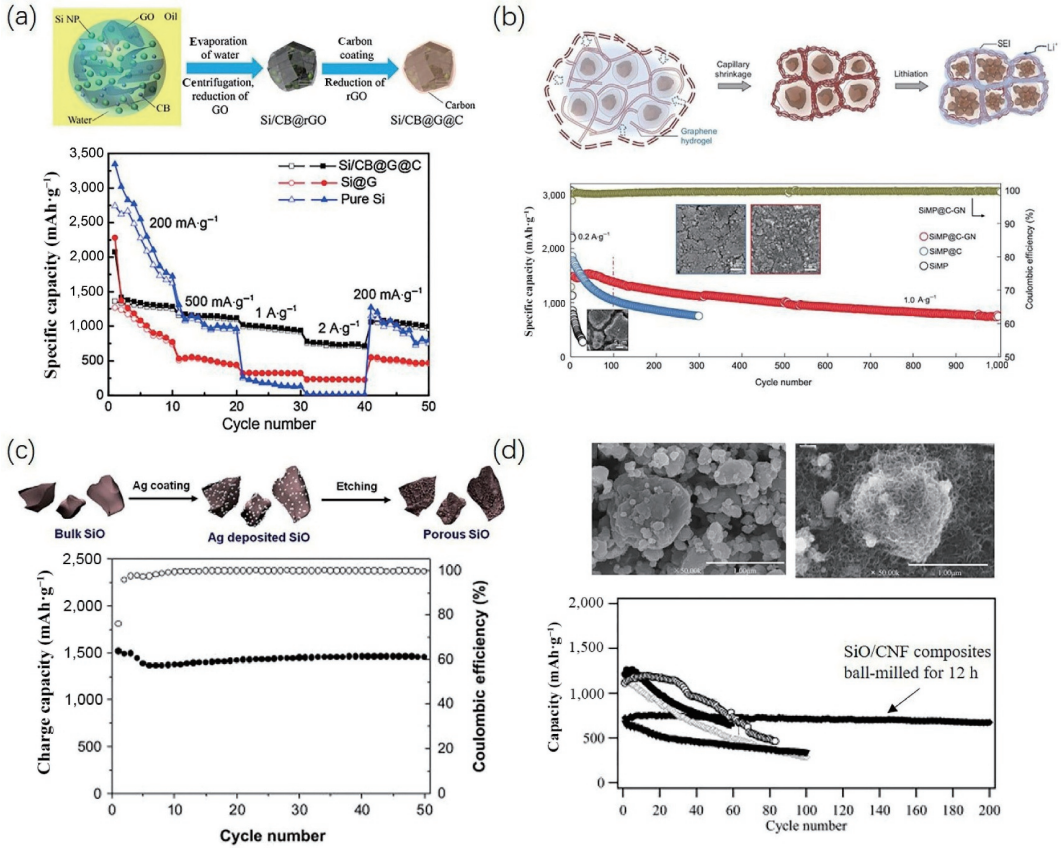

Figure 6 Carbon coating strategies for silicon-based materials. (a) Schematic of the preparation process of Si/CB@G@C and rate capability of Si/CB@G@C, Si@G, and pure Si. Reproduced with permission from Ref. [75], © Elsevier Ltd. 2016. (b) The formation of 3C architecture in SiMP@C-GN and cycling stability of SiMP@C-GN anode. Reproduced with permission from Ref. [100], © Chen, F. Q. et al. 2021. (c) Schematic illustration of the synthetic route for preparing the porous SiO using Ag catalytic etching and its cycling performance. Reproduced with permission from Ref. [101], © Elsevier Ltd. 2012. (d) SEM images of SiO and SiO/CNF composites ball-milled for 12 h with the cycling performance. Reproduced with permission from Ref. [102], © Elsevier B.V. 2011.

At present, the main methods of carbon coating for SiO_x include CVD [101, 103–105] and ball milling [102, 106]. Through galvanic displacement reaction and metal catalytic etching process with Ag, porous SiO was acquired by Park and his coworker. Then, acetylene-derived carbon coating was formed by CVD. Benefiting from the combination of porous structures and carbon coating, the volume expansion of this composite was greatly suppressed, thus a considerable capacity of 1,490 $mAh·g^{-1}$ over 50 cycles was sustained at 0.1 C (Fig. 6(c)) [101]. Takeda et al. used HEMM to prepare micron size SiO powder and mixed it with carbon nanofiber (CNF) [102]. The composite with particle sizes of 0.1–1 μm showed good cycling performance due to the nanosized SiO and a low content of SiO_2. Therefore, an outstanding cycling performance with a high reversible capacity of ~ 675 $mAh·g^{-1}$ was remained after 200 cycles (Fig. 6(d)).

Generally, heat treatment conditions of the carbon coating strategy such as heating time, heating temperature, and atmosphere have effects on the formation of Si-based anode and thus indirectly affect the electrochemical properties. Hou et al. systematically evaluated the electrical performance of the disproportionated SiO (D-SiO) and graphene-coated SiO (SiO@G) under different heat treatment conditions [107]. With the increase of heating time and temperature, D-SiO underwent a disproportionation reaction by forming Si and SiO_2. The thicker SiO_2 shell prevented Li^+ ions from passing through, leading to severe overpotential and poor cycling life. For SiO@G, the graphene coating effectively constrained the growth of SiO_2 shell and protected the SiO surface. Such a protective layer achieved a high ICE (79.3%) and long cycling stability (84.2% after 200 cycles).

Although rigid carbon coating provides a fast transmission pathway for lithium ions and electrons, it is not sufficient to maintain the structural integrity of the electrodes. As a result, flexible coatings (also known as elastic coatings) with good mechanical properties afford flexibility to assist in accommodating Si/SiO_x volume change during cycles, leading to highly sustainable cycling performance with high capacity. In one example, Hyun et al. encapsulated SiNPs in bacterial cellulose and constructed a functional barrier coating of polyaniline (PANI) on the surface of SiNPs by using phytic acid to increase the adhesion of aniline monomers to SiNPs [108]. Consequently, the 3D flexible conductive composite maintained stable electrical conductivity in the bending testing and showed great potential as an anode for flexible rechargeable batteries. In another example, Guo et al. developed a stable and flexible interface with good conductivity on the carbon-coated SiO_x microparticles (SiO_x/C) via *in-situ* polymerization of Li poly(acrylic acid) (LiPAA) , followed by blended with carbon nanotubes [109]. The elastic LiPAA interface changed dynamically with the expansion and contraction of SiO_x/C during (de)lithiation processes, avoiding the disintegration of SiO_x particles and the overgrowth of SEI. The as-prepared SiO_x/C with flexible Li-PAA interface achieved superior cycling performance of 836 $mAh·g^{-1}$ after 500 (de)lithiation processes, better than the original SiO_x/C anode (458 $mAh·g^{-1}$).

2.2.2 *Metal and metal oxide coating*

Due to the high electrical conductivity, excellent ductility, and mechanical strength of metals, metal coating as a protective layer is an ideal strategy for mitigating volume change and improving electrical conductivity. Up to date, various metals have served as buffer matrixes, such as Ag [110], Ge [111], and Cu [112]. Ensafi et al. prepared porous silicon by chemical etching Ag particles

deposited on the surface of Si [76]. Then, Ni@PSiF or Bi@PSiF composite was fabricated by the deposition of Ni or Bi nanoparticles on the surface of Si via an electroless method in the presence of F^- ions. Due to the high surface area of PSiF and the high conductivity of Ni and Bi particles, both Ni@PSiF and Bi@PSiF achieved large initial specific capacity of 2,500 and 3,200 mAh·g^{-1} and high ICE of 98% and 97%, respectively. Besides, both of them demonstrated good cycling performance at 400 mA·g^{-1} after 100 cycles.

Yang et al. developed a liquid metal (LM: Ga 90 wt.% and In 10 wt.%) coating method and combined with CVD process on SiMPs (denoted as Si/LM@C-CNF) to resolve the expansion and polarization of Si particles during cycling [113]. LM coating as an electrically conducting medium connected between inner SiMPs and outer carbon shell, effectively buffered the electrode deformation, and improved electrical conductivity. The composite maintained large volume specific capacity of 936 mAh·cm^{-3} at 5 A·g^{-1} over 150 cycles (Fig. 7(a)). Meanwhile, Kim et al. prepared a nanostructured $SiAl_{0.2}O$ composite material consisting of silicon nanocrystallites (< 10 nm in size) via HEMM process [114]. The electrochemically inactive Al component could replace part of the SiO_2 and improve mechanical strength properties, which greatly restrained the pulverization of SiO particles upon lithiation/delithiation process. As a result, $SiAl_{0.2}O$ electrode exhibited an increase of 10% in ICE compared with SiO and improved cycling performance, showing a capacity of 800 mAh·g^{-1} at the end of 100th cycle (Fig. 7(b)).

The external metallic oxides (MO) protective layer not only alleviates the volume expansion of Si/SiO_x particles upon lithiation/delithiation proceed, but also impedes the corrosion of electrolyte to internal Si/SiO_x particles, thus retaining the structural integrity of Si/MO composites and improving cycle stability. The common metallic oxides coating materials include TiO_2 [79], Al_2O_3 [115, 116], zeolites [117], and so forth. For example, Liu et al. demonstrated Si@a-TiO_2 core–shell structure by a simple sol-gel approach [79]. The SiNPs were wrapped by amorphous titanium oxide (a-TiO_2) which had lower Li^+ diffusion energy. More importantly, the flexible and elastic TiO_2 shells remained undamaged during discharge and charge process. Besides, the stable SEI film was formed on the surface of a-TiO_2 to prevent the electrolyte from penetrating into the Si core. Hence, the Si@a-TiO_2 as anodes for LIBs manifested a high ICE of ~ 86.1% and a large reversible capacity of 1,720 mAh·g^{-1} at 420 mA·g^{-1} (Fig. 7(c)). Similarly, TiO_2 coating layer is also of great importance to SiO_x-based anode for LIBs. Jeong et al. explored a facile sol-gel process of using titanium iso-propoxide as precursor and heating at 400 °C to prepare a SiO@TiO_2 anode [118]. TiO_2 shell could retard thermal runaway and improve the safety of LIBs. SiO@TiO_2 anode showed a better capacity of over 1,000 mAh·g^{-1} than that of pristine SiO with a high energy density of 684 Wh·L^{-1}.

2.2.3 *Polymer coating*

Apart from metal coating, polymer coating (especially conductive polymers) is also feasible in relieving fracture of Si/SiO_x particles. Polymers have the advantages of flexibility and elasticity and act as the flexible medium to mitigate the volume changes during cycling, endowing Si or SiO_x with the ability to self-healing. PANI [119], polypyrrole (PPy) [120], and poly(3,4-ethylenedioxythiophene) (PEDOT) [120, 121] are commonly used conductive polymers for high-performance LIB anodes. Wu et al. synthesized a composite microsized Si anode (PCSi-2) with coating of poly(hexaazatrinaphthalene) (PHATN) [122]. During the cycling, PHATN went through the molecular transformation configuration, forming free space to accommodate the volume

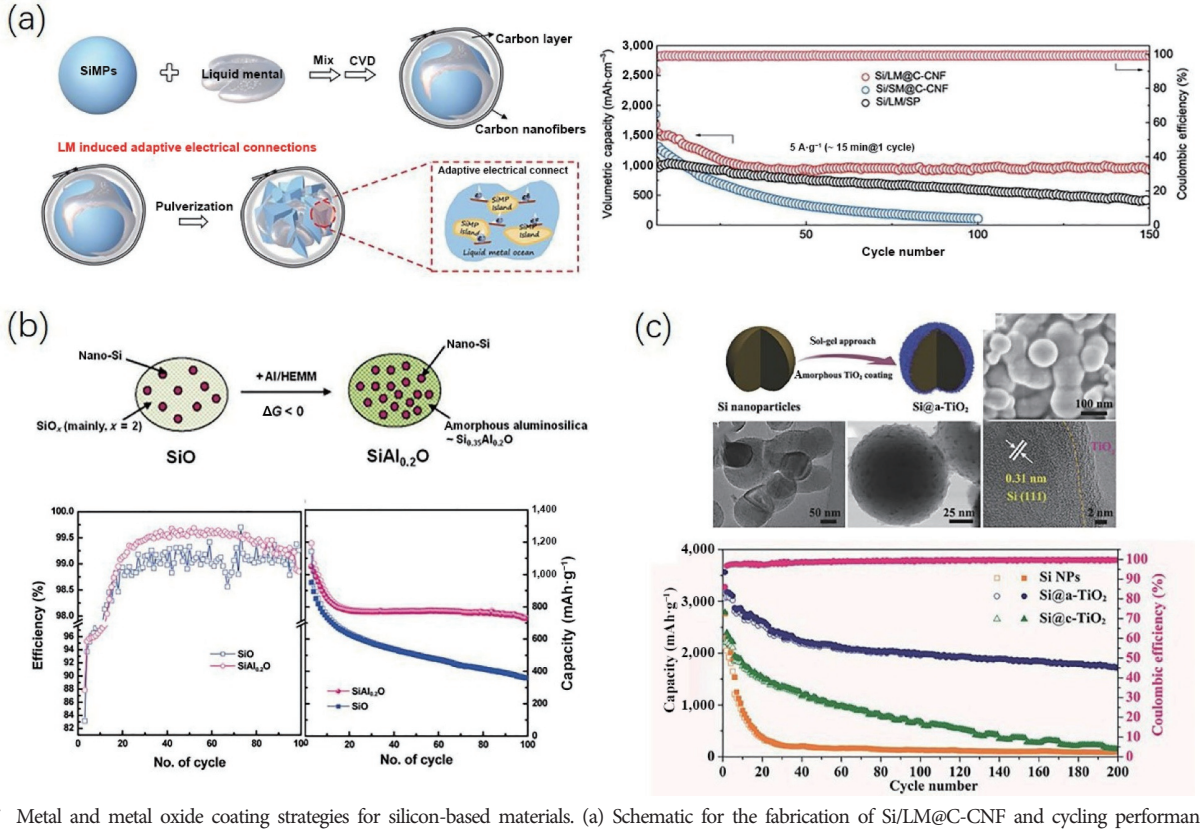

Figure 7 Metal and metal oxide coating strategies for silicon-based materials. (a) Schematic for the fabrication of Si/LM@C-CNF and cycling performances of Si/LM@C-CNF, Si/SM@C-CNF, and Si/LM/SP at 5 A·g^{-1}. Reproduced with permission from Ref. [113], © Wiley-VCH 2022. (b) Schematic illustration of nanostructured $SiAl_{0.2}O$ material and its cycling performance. Reproduced with permission from Ref. [114], © American Chemical Society 2010. (c) Schematic illustration of fabrication process for the amorphous-TiO_2-coated Si core–shell nanoparticles and cycling performance of the pristine Si, Si@a-TiO_2, and Si@c-TiO_2. Reproduced with permission from Ref. [79], © WILEY-VCH Verlag GmbH & Co. KGaA, Weinheim 2017.

expansion. Along with the sodium alginate (SA) binder, a strong self-healing hydrogen bond networks generated, forming a robust and stable structure. Consequently, PCSi-2 composite showed a long and stable cycle life over 500 cycles at 1 A·g^{-1} with a high reversible capacity of 1,129.6 mAh·g^{-1} (Fig. 8(a)). Zhu et al. reported a unique SiO structure with a C/polymer bilayer coating (Si-SiO$_x$@C/CNP-PPy; CNP-PPy = C-nanoparticle-reinforced polypyrrole) [123]. Through the thermal decomposition of phenolic resin and microwave thermolysis of honey followed by the polymerization from pyrrole to PPy, the internal C layer and the external CNP-PPy were produced, respectively. The conductive and flexible bilayer coating not only improved electrical conductivity but also enhanced structural stability. The new design of electrode exhibited a large ICE of 69.8% and a high capacity retention of 83% at 2 C after 900 cycles (Fig. 8(b)).

2.2.4 *Surface functionalization/artificial solid electrolyte interface*

Surface functionalization has demonstrated an effective way to decrease the side reaction between Si-based anodes and electrolytes. As a result, a stable and robust protective layer can be constructed on the surface of Si/SiO$_x$ particles. For example, SiNPs were surface-modified with epoxy group treated by hydrogen peroxide (H_2O_2) to enrich the Si–OH group and followed by a silanization reaction with the epoxy-containing silane precursor [124]. The epoxy group of the functionalized SiNPs prevented the direct contact between the SiNPs and electrolytes. Moreover, the formation of covalent bonding between the epoxy group and the hydroxyl group in the poly(acrylic acid) binder maintained the structural integrity of SiNPs. Thus, the electrode with epoxy group showed improved cycling performance and higher CE than the pristine SiNPs during (de)lithiation processes. Wang et al. synthesized three different functional groups including silanol silicon (Sis), carboxyl silicon (Sic), and siloxane silicon (Sio) on the surface of commercial SiNPs through different chemical treatment [125]. For Sis and Sic, the SEI layers were easily cracked, leading to the serious capacity fade, yet the Sio-contained SiNPs had a stable SEI layer and a longer cycling life. In addition to surface functionalization, artificial SEI (ASEI) with superior ion conductivity, mechanical strength, and good flexibility can protect the Si-based anode from reactions with chemicals in the organic solvent, and thus significantly improve the cycling stability. Cui et al. demonstrated an artificial SEI (Li$_x$Si coated by LiF and lithium decylcarbonate) via mechanical stir and heat treatment, followed by mixing Li$_x$Si NPs and 1-fluorodecane in anhydrous cyclohexane [126]. The protective ASEI layer coated on SiNPs provided accommodations for volume changes and sufficient Li source. Therefore, the ICE was increased (76.1% to 96.8%) and corresponding cycling life was extended to 100 cycles. Furthermore, Wang et al. designed a porous SiO coated with polytannins (PTN) by *in-situ* polymerization of tannin in NaOH solution [127]. The ASEI effectively hindered the volume expansion of the porous SiO and prevented pulverization during cycling processes. The as-prepared SiO anode obtained a longer cycling life and higher ICE than pristine porous SiO$_x$. Moreover, the performances of recently developed nanostructured and surface engineered Si-based anodes are summarized in Table 1.

2.3 Novel binders

In addition to optimizing the silicon-based materials themselves, the advanced design of polymer binders plays a vital role in constructing stable silicon-based anodes as well [128–132]. There are mainly two roles of effective polymeric adhesive: (1) to provide adhesion and cohesion for active and inactive ingredients; and (2) to bond the materials with a current collector. Reasonable design of polymer binders with high bonding strength can effectively sustain the mechanical integrity of the anode, prevent the electrode–electrolyte reaction, relieve the volume expansion of Si/SiO$_x$ particles, and inhibit the structural degradation [133–135]. Polymer binders for silicon-based anodes can be classified into three types in terms of the polymer structures: linear, branched, and crosslinked polymers.

2.3.1 *Linear polymer binders*

In general, linear polymers are continuous long chains consisting of carbon–carbon bonds with few branches between the chains. The molecular weight (M_W) and side groups can determine the binding ability [136, 137]. The most common polymer binders include sodium carboxymethyl cellulose (CMCNa) [138], alginate (Alg) [139], chitosan (CS) [140], PAA [141, 142], and so forth.

CMC is a derivative of cellulose, containing repeated hydroxyl groups (–OH) and carboxymethyl (–OCH$_2$COONa) groups. In conventional graphite anodes, CMC/styrene-butadiene rubber (SBR) composite binder is the most widely used binder. Early studies have found that it might be a good adhesive for silicon-based anodes in terms of the advantages of environmentally benignity and low lost compared with poly(vinylidene fluoride)

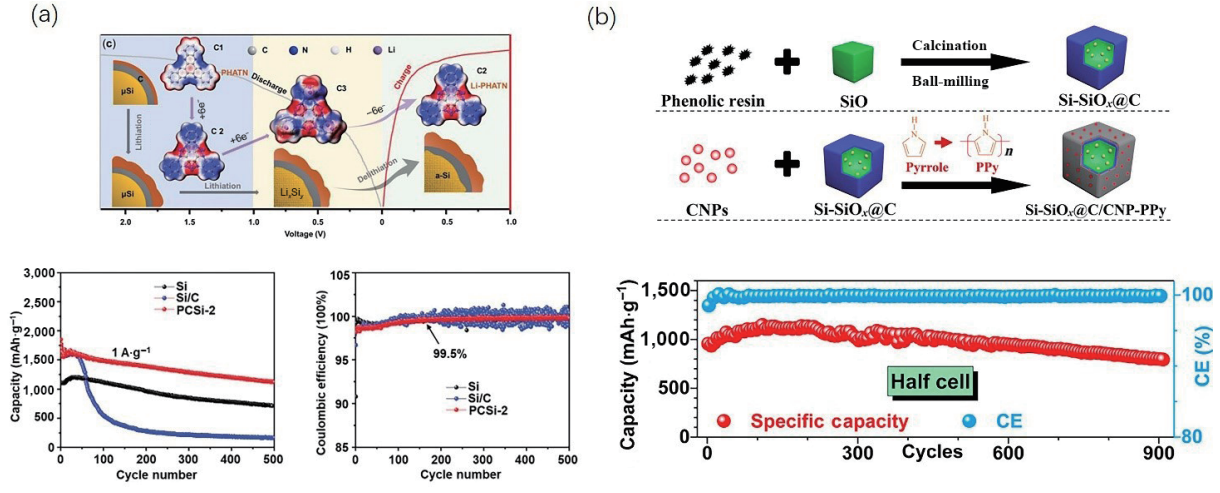

Figure 8 Polymer coating strategies for silicon-based materials. (a) Schematic illustration of microscopic structural evolution of PCSi-2 electrode during the charging/discharging process and distribution of electrostatic potential (ESP) of PHATN at different states; cycling stability and corresponding Coulombic efficiency of PCSi-2. Reproduced with permission from Ref. [122], © Wiley-VCH GmbH 2022. (b) Schematic of the experimental procedure for synthesizing Si-SiO$_x$@C/CNP-PPy particles and its cycling performance. Reproduced with permission from Ref. [123], © American Chemical Society 2020.

Table 1 Recent progresses on Si-based anodes with various structure engineering strategies

No.	Electrode	1st cycle	Long cycling performance	References
1	Si nanoparticles	3,530 mAh·g^{-1} with 82% CE at 0.179 mA·g^{-1}	2,200 mAh·g^{-1} after 250 cycles at C/7	[143]
2	Si NWs	4,125 mAh·g^{-1} with 76% CE at 1/16 C	3,302 mAh·g^{-1} after 100 cycles at 1 C	[42]
3	Si/Cu NW	2,854.4 mAh·g^{-1} with 93.1% CE at 0.1 C	1,488 mAh·g^{-1} after 100 cycles at 1 C	[144]
4	Nonporous SiNW	4,000 mAh·g^{-1} with 83% CE at 0.1 C	2,000 mAh·g^{-1} after 250 cycles at 0.5 C	[43]
5	Si nanosheets	875 mAh·g^{-1} with 61.6% CE at 0.1 A·g^{-1}	721 mAh·g^{-1} after 1,800 cycles at 0.1 A·g^{-1}	[41]
6	Si/ZnO/C nanosheets	1,761 mAh·g^{-1} with 80.3% CE at 500 mA·g^{-1}	1,536 mAh·g^{-1} after 800 cycles at 1.0 A·g^{-1}	[40]
7	Silicene flowers	3,182 mAh·g^{-1} with 74% CE at 200 mA·g^{-1}	1,100 mAh·g^{-1} after 600 cycles at 2 A·g^{-1}	[57]
8	Si@C	2,395 mAh·g^{-1} with 67.5% CE at 0.1 A·g^{-1}	1,120 mAh·g^{-1} after 500 cycles at 2 A·g^{-1}	[145]
9	Si@graphene	2,842.9 mAh·g^{-1} with 85.5% CE at 1.8 A·g^{-1}	800 mAh·g^{-1} after 150 cycles at 1.8 A·g^{-1}	[39]
10	Si/C nanosphere	1,421 mAh·g^{-1} with 66% CE at 0.2 A·g^{-1}	738 mAh·g^{-1} after 120 cycles at 0.4 A·g^{-1}	[88]
11	Si@N/C	1,697 mAh·g^{-1} with 67.4% CE at 200 mA·g^{-1}	603 mAh·g^{-1} after 120 cycles at 200 mA·g^{-1}	[146]
12	R-YS Si/C spheres	1,100 mAh·g^{-1} with 78.6% CE at 200 mA·g^{-1}	981 mAh·g^{-1} after 250 cycles at 200 mA·g^{-1}	[147]
13	CNT@Si@C	810 mAh·g^{-1} with 84% CE at 0.1 mA·cm^{-2}	690 mAh·g^{-1} after 500 cycles at 0.75 mA·cm^{-2}	[148]
14	Si/CB@G@C	1,380 mAh·g^{-1} with 66.4% CE at 0.2 A·g^{-1}	908 mAh·g^{-1} after 50 cycles at 200 mA·g^{-1}	[75]
15	W-Si@N-CNFs	1,490 mAh·g^{-1} with 69% CE at 200 mA·g^{-1}	658 mAh·g^{-1} after 150 cycles at 200 mA·g^{-1}	[149]
16	Check-Cu/Si	988 mAh·g^{-1} with 25% CE at 6 A·g^{-1}	359 mAh·g^{-1} after 200 cycles at 6 A·g^{-1}	[150]
17	Si-$FeSi_2$-G-C	1,045 mAh·g^{-1} with 87% CE at 0.2 A·g^{-1}	925 mAh·g^{-1} after 80 cycles at 200 mA·g^{-1}	[82]
18	Cu-Si NW@Al_2O_3	998 mAh·g^{-1} with 88% CE at 3 A·g^{-1}	705 mAh·g^{-1} after 800 cycles at 3 A·g^{-1}	[50]
19	Si@TiO_2@RGO	2,815.6 mAh·g^{-1} with 83% CE at 1.4 A·g^{-1}	1,679 mAh·g^{-1} after 900 cycles at 1.4 A·g^{-1}	[151]
20	Hollow Si	3,795.3 mAh·g^{-1} with 72.3% CE at 0.1 A·g^{-1}	779 mAh·g^{-1} after 1,100 cycles at 8 A·g^{-1}	[59]
21	Hollow Si nanocubes	1,728 mAh·g^{-1} with 80.1% CE at 0.1 A·g^{-1}	850 mAh·g^{-1} after 800 cycles at 1 C	[80]
22	Hollow SiO_2/C	1,300 mAh·g^{-1} at 0.1 A·g^{-1}	802 mAh·g^{-1} after 300 cycles at 200 mA·g^{-1}	[152]
23	Hollow p-Si@C	2,400 mAh·g^{-1} with 79% CE at 0.1 A·g^{-1}	1,869 mAh·g^{-1} after 250 cycles at 1.2 A·g^{-1}	[153]
24	Hollow Si@SnO/C	2,023 mAh·g^{-1} with 74.3% CE at 500 mA·g^{-1}	1,535 mAh·g^{-1} after 200 cycles at 0.5 A·g^{-1}	[154]
25	Hollow Si/C/void/SiO_2/C	1,641 mAh·g^{-1} with 64% CE at 100 mA·g^{-1}	900 mAh·g^{-1} after 100 cycles at 100 mA·g^{-1}	[61]
26	Hollow Ni/SiO_2	676 mAh·g^{-1} with 56.6% CE at 0.1 A·g^{-1}	337 mAh·g^{-1} after 1,000 cycles at 10 A·g^{-1}	[155]
27	Porous micro-Si	2,500 mAh·g^{-1} with 75% CE at 0.26 A·g^{-1}	1,218 mAh·g^{-1} after 370 cycles at 2.6 A·g^{-1}	[156]
28	Porous Si/C	916 mAh·g^{-1} with 64% CE at 0.05 A·g^{-1}	418 mAh·g^{-1} after 200 cycles at 0.5 A·g^{-1}	[157]
29	Porous C/Si-rGO-Si/C	1,553 mAh·g^{-1} with 68% CE at 200 mA·g^{-1}	1,187 mAh·g^{-1} after 200 cycles at 1 A·g^{-1}	[97]
30	Porous N-PSi@C	3,188 mAh·g^{-1} with 93.8% CE at 0.05 C	1,200 mAh·g^{-1} after 500 cycles at 7 C	[94]
31	Porous NPC@Si	2,504 mAh·g^{-1} with 84% CE at 0.5 A·g^{-1}	1,565 mAh·g^{-1} after 100 cycles at 0.5 A·g^{-1}	[89]
32	Porous Si-Ge	1,951 mAh·g^{-1} with 75.6% CE at 0.1 A·g^{-1}	1,158 mAh·g^{-1} after 150 cycles at 1 A·g^{-1}	[158]
33	Core–shell Si/C	620 mAh·g^{-1} with 89.2% CE at 0.1 C	620 mAh·g^{-1} after 500 cycles at 0.5 C	[159]
34	Core–shell Si@N	2,602 mAh·g^{-1} with 75.4% CE at 420 mA·g^{-1}	725 mAh·g^{-1} after 100 cycles at 420 mA·g^{-1}	[92]
35	Core/shell Si/Ge NW	2,133 mAh·g^{-1} with 87.5% CE at 800 mA·g^{-1}	1,710 mAh·g^{-1} after 10 cycles at 4 A·g^{-1}	[160]
36	Core/shell Ge@aSi NWs	1,996 mAh·g^{-1} with 79.8% CE at 0.2 C	1,455 mAh·g^{-1} after 150 cycles at C/5	[161]
37	Core–shell porous Si@graphene	2,379 mAh·g^{-1} with 77.8% CE at 0.1 A·g^{-1}	1,124 mAh·g^{-1} after 120 cycles at 0.4 A·g^{-1}	[162]
38	Core–shell SiO_x-TiO_2@C	1,011 mAh·g^{-1} with 62.5% CE at 0.1 A·g^{-1}	910 mAh·g^{-1} after 200 cycles at 0.1 A·g^{-1}	[163]
39	Core–shell NCNTs-Ni_2Si@porous Si	1,956 mAh·g^{-1} with 80.9% CE at 358 mA·g^{-1}	1,315 mAh·g^{-1} after 600 cycles at 0.1 C	[58]
40	Core–shell Si-Mn/C	793 mAh·g^{-1} with 49.6% CE at 0.1 A·g^{-1}	960 mAh·g^{-1} after 100 cycles at 1 A·g^{-1}	[83]
41	Core–shell Si@void@NGS	2,000 mAh·g^{-1} with 68% CE at 1 A·g^{-1}	1,775 mAh·g^{-1} after 750 cycles at 1 A·g^{-1}	[164]
42	Core–shell Si@void@C	1,700 mAh·g^{-1} with 62.1% CE at 0.2 A·g^{-1}	854 mAh·g^{-1} after 200 cycles at 0.2 A·g^{-1}	[90]
43	Core–shell Si@a-TiO_2	3,061 mAh·g^{-1} with 86.1% CE at 140 mA·g^{-1}	1,720 mAh·g^{-1} after 200 cycles at 420 mA·g^{-1}	[79]

(PVdF) binder. Zhang et al. revealed that CMC could dramatically improve the cyclic stability of SiO_x/graphite electrode because it did not react with the electrolyte and could form chemical bonds with active materials. Therefore, SiO_x/graphite anode with CMC binder exhibited low impedance, high ICE of 77.92%, and good rate capability [165]. Furthermore, the binding ability of CMC binder is related to its molecular weight and the degree of substitution (DS, the number of carboxymethyl group per unit) by the carboxymethyl group. Liu et al. prepared CMC binder with different DS via a repeated process of alkalization with NaOH and

etherification with sodium chloroacetate [166]. The anode with the CMC binder when DS was equal to 0.55 achieved the excellent electrochemical performance owing to the synergistic effect of covalent bonds and hydrophobic bonds. As a consequence, the anode with CMC binder (DS = 0.55) showed the higher specific capacity of 1,407 mAh·g^{-1} after 100 cycles than those with lower or higher DS.

In addition to CMC, another naturally occurring polymer, sodium Alg, is also widely employed as a Si-based binder. For example, Choi and coworkers reported an amphiphilic binder with a hydrophobic protein acting as backbone and hydrophilic oligosaccharide as branches [167]. Because of two functional components, the renatured DNA-alginate (reDNA/Alg) binder with 3D network structure exhibited amphiphilicity and promoted uniform distribution of electrode components. The strong adhesion further avoided the binder peeling off the current collector and improved cyclability for silicon-based LIBs. Therefore, the anode with reDNA/Alg binder showed high capacity retention of 80.1% after 160 cycles at high current density of 1,750 mA·g^{-1} compared with reDNA or Alg binder (Fig. 9(a)). In 2010, PAA was first reported by Yushin et al. as a binder for SiNP anodes [168]. PAA film had similar swelling and mechanical properties to CMC binder. PAA binder can effectively raise the cyclability of SiNP anodes due to its high concentration of carboxylic groups (–COOH) which enhances the adhesion between Si particles. Komaba et al. found that the best electrochemical performance was achieved by applying PAA as the binder compared to the PVdF, CMCNa, and poly(vinyl alcohol) (PVA) binders [141]. The flexible PAA polymer not only connected SiO particles, but accommodated the volume changes of the anode upon lithiation. The reversible capacity of SiO with the PAA binder reached up to 700 mAh·g^{-1} after 50 cycles at 100 mA·g^{-1} (Fig. 9(b)).

Blending PAA with other polymers, such as CMC [169], pullulan [170], pectin [171], polyvinyl butyral [172], PVA [173, 174], polyaniline [175], and Nafion [176], can achieve better performance than the individual polymers owing to the combination of merits of PAA and other polymers. For instance, Wang et al. synthesized water-soluble glycinamide modified PAA (PAA-GA) via a coupling method by adding N-(3-dimethylaminopropyl)-N'-ethylcarbodiimide hydrochloride (EDC) and N-hydroxysuccinimide (NHS) to form chemical bonds as a polymer binder for silicon anodes to alleviate its massive volume expansion [177]. The PAA-GA-based silicon electrodes possessed a high capacity retention of 81% after 285 cycles with a high average Coulombic efficiency of 86.5% (Fig. 9(c)). Another example, a novel pectin/PAA (PEC/PAA) blend binder with reversible elasticity through simple physical mixing and drying was developed by Hong and coworkers to suppress the massive volume change of SiNPs [178]. The intrinsic functional groups (–OH, –COOH, and –(C=O)OCH$_3$) of PEC interacted with PAA to form a hydrogen-bonded 3D physical network. When the weight fraction of PEC was 10%, PEC/PAA binder had good mechanical strength and adhesion, resulting in superior electrochemical performances compared with PAA alone.

2.3.2 *Branched polymer binders*

A branched polymer can be regarded as a macromolecule containing a large number of repeating groups arranged in a branched structure. The properties of branched polymers mainly depend on the amount of branching. PAA is the most widely studied structure units in the construction of branched polymer adhesives for high-performance Si anodes. Saito et al. synthesized a graft copolymer binder by two reaction methods, the first method was through the amidation reaction of glycol chitosan (GC) to prepare macro-RAFT-CTA (RAFT: reversible addition-fragmentation chain transfer, CTA: chain transfer agent) and then a RAFT polymerization was carried out by acrylic acid, 4,4'-

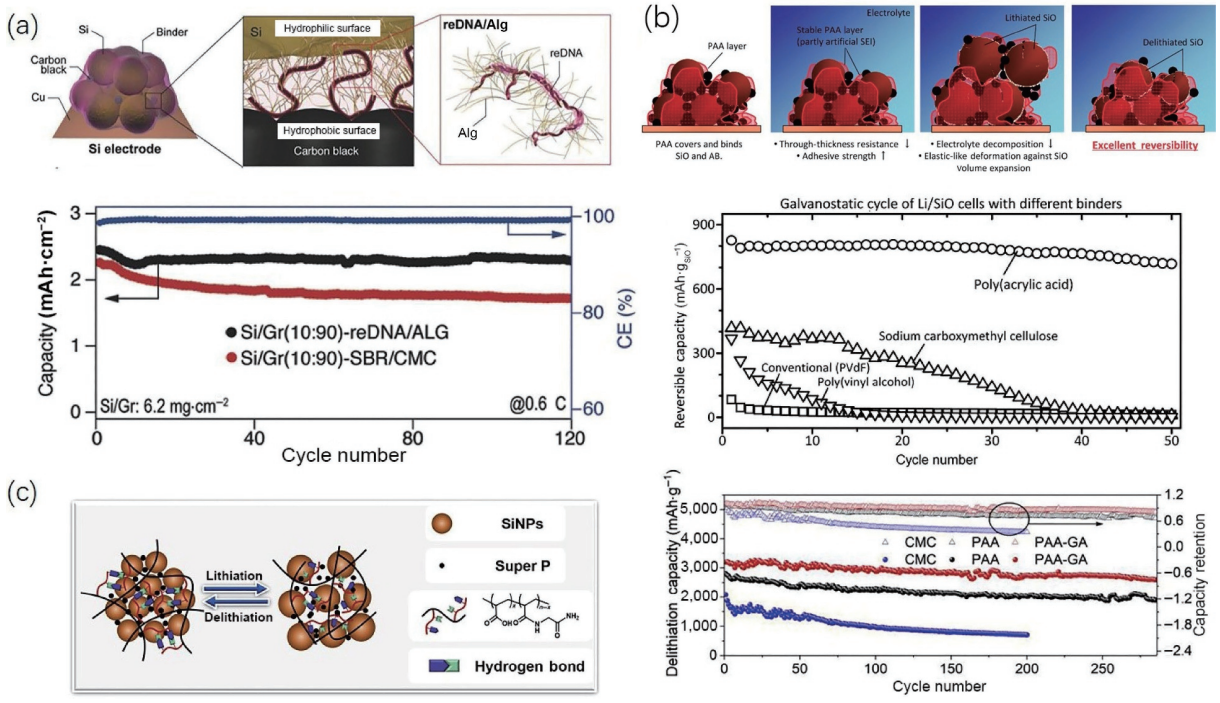

Figure 9 Linear polymer binders for silicon-based materials. (a) The proposed reDNA/Alg hybrid binder at Si/carbon interfaces and cycling performance of Si/Gr (10:90) anodes with reDNA/Alg and CMC/SBR binders at 0.6 C. Reproduced with permission from Ref. [167], © WILEY-VCH Verlag GmbH & Co. KGaA, Weinheim 2018. (b) Schematic illustrations of the proposed mechanism for the improved cyclability for the SiO powder composite electrodes and cycling performance of SiO anodes with different binders. Reproduced with permission from Ref. [141], © American Chemical Society 2011. (c) Schematic illustration of the lithiation/delithiation process of silicon electrode using PAA-GA polymer as binder and cycling performance and capacity retention of the electrodes with different binders. Reproduced with permission from Ref. [177], © Elsevier B.V. 2018.

azobis(4-cyanopentanoic acid), and LiOH to produce GC-g-LiPAA [179]. The silicon/graphite composite anode with GC-g-LiPAA binder revealed increased initial discharge capacity, and high capacity retention and Coulombic efficiency (Fig. 10(a)). Chitosan-g-poly(acrylic acid) copolymer (CS-PAA) and its sodium salt (CS-PAANa) were produced by Yu and coworkers through a simple graft polymerization [180]. The crosslinked functional groups contributed to the construction of the robust 3D network during curing. Both –COOH and –COO– groups reacted with –OH groups on the surface of Si particles and Cu foil to form covalent bonds, ensuring the electrode integrity during the repeated insertion and extraction of lithium process, and greatly increased the stability of Si anodes. As a result, both Si/CS-PAA and Si/CS-PAANa electrodes exhibited outstanding specific capacities of ~ 1,240 and ~ 1,600 mAh·g^{-1} at 420 mA·g^{-1} after 100 cycles, respectively (Fig. 10(b)).

2.3.3 *Crosslinked polymer binders*

Crosslinked polymers often have two or more polymer chains connected together at one or more points other than their ends. The interconnected network linked by numerous covalent bonds improves the mechanical and physical properties of the crosslinked polymer. Crosslinked structure can reduce the severe mechanical stress caused by the huge volume change, avoid active materials peeling off the current collector, and maintain the structural integrity of the electrode [181–188]. For example, Zhang et al. prepared a dual cross-linked network binder by emulsion polymerization of different polymers to form fluoropolymer (FP) followed by thermal polymerization between the fluorinated copolymer and sodium alginate (denoted as FPSA) [189]. The chemical and physical cross-linked FPSA binder could effectively protect the SiNPs during the cycling process. Consequently, a high capacity of 1.557 mAh·g^{-1} was remained at 4 A·g^{-1} after 200 cycles by employing this dual functional binder (Fig. 11(a)). Moreover, Chen et al. successfully applied a cross-linked hyperbranched polyethylenimine (PEI) with complicated 3D network as an effective adhesive for Si-based LIBs [190]. The highly crosslinked PEI could interact with SiO at the surface of silicon to construct robust H-bonding networks and effectively buffer large volumetric change of silicon particles, thus the integrity of the anode could be preserved during lithiation/delithiation process. This crosslinked polymer delivered a considerable initial discharge capacity of ~ 3,800 mAh·g^{-1} with high ICE of 91.6%, and still sustained 2,180 mAh·g^{-1} after 100 cycles (Fig. 11(b)). Zheng et al. prepared a crosslinked polymer binder (SA-PAA) by esterification reaction between PAA and SA [191]. The as-prepared binder could adapt the volume expansion of sub-micro Si particles in the process of continuous charging and discharging. The electrode with SA-PAA binder had higher initial Coulombic efficiency, cycle performance, and rate performance compared with those with SA and PAA binders.

Dou and coworkers developed a polydopamine grafted crosslinked polyacrylamide (PDA-c-PAM) via dissolving dopamine in NaOH aqueous solution followed by adding N,N'-methylenediacrylamide, ammonium persulfate, and tetramethylenediamine to acrylamide solution under an inert atmosphere [192]. The PDA side chain had superior adhesion to SiO and current collector and the PAM main chain could accommodate the large volume change. SiO/graphite with the PDA-c-PAM binder delivered a large initial discharge capacity of 1,350 mAh·g^{-1} and maintained 591 mAh·g^{-1} at 1 A·g^{-1} after 300 cycles with an average capacity fading rate of 0.27% per cycle. A summary of different polymer binders for Si-based anodes and their long cycling performances are shown in Table 2.

2.4 Innovative design of electrolytes

Besides novel binders, electrolyte is another significant factor that impacts the electrochemical properties of silicon-based LIBs [193–196]. SEI, a passivation layer, is considered as an important role in LIBs. During charge and discharge process, SEI is generated on anode surfaces from decomposition products of electrolytes. However, the SEI film is continuously cracked and reformed arising from the repeated volume change of Si-based electrodes [197–202]. Therefore, constructing a stable and robust SEI film can homogenize the mechanical stress and strain during continuous lithiation/delithiation process of Si/SiO$_x$ particles to constrain their expansion and contraction and protect the SEI from crumbling. A great many novel solvents, electrolyte

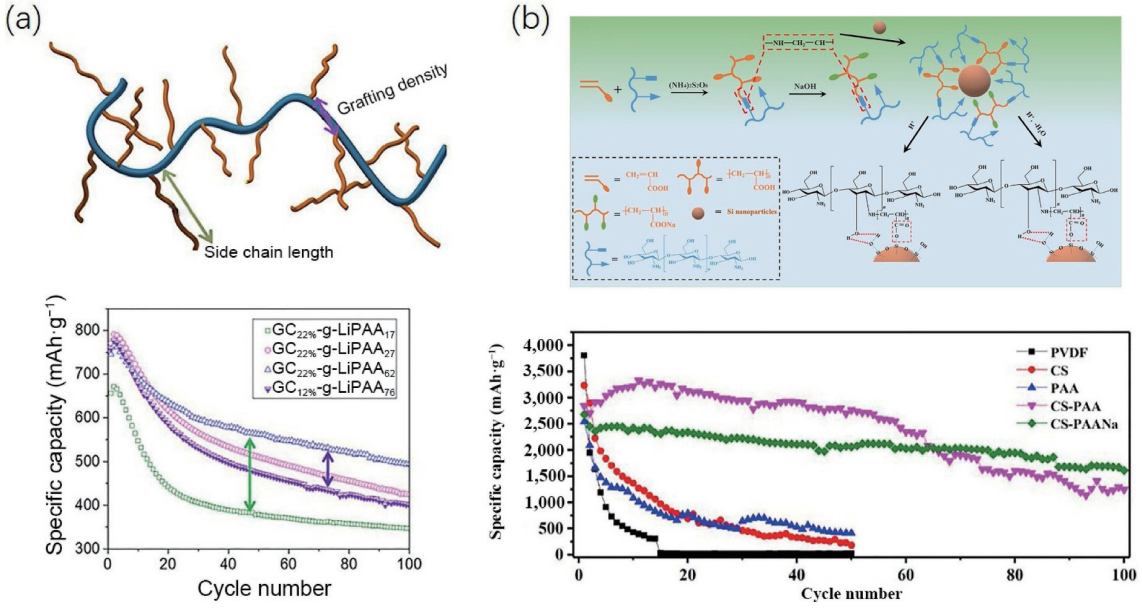

Figure 10 Branched polymer binders for silicon-based materials. (a) Graft copolymer GC-g-LiPAA and cycling performance of silicon/graphite electrodes at 0.1 C. Reproduced with permission from Ref. [179], © American Chemical Society 2018. (b) Scheme for the preparation of CS-PAA and CS-PAANa and proposed bonding mechanism between binders and Si nanoparticles; the cycling performance of electrodes at 420 mA·g^{-1}. Reproduced with permission from Ref. [180], © American Chemical Society 2019.

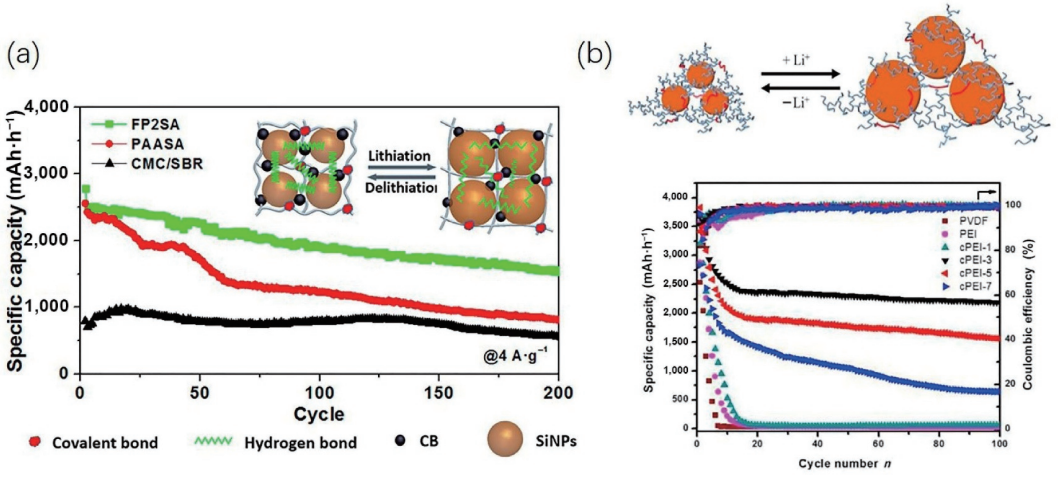

Figure 11 Crosslinked polymer binders for silicon-based materials. (a) Schematic representations of Si based binder configurations for the dual cross-linked binder during lithiation/delithiation and cycling performance of Si-based electrodes with different binders at 4 A·g^{-1}. Reproduced with permission from Ref. [189], © American Chemical Society 2019. (b) Illustration of charge/discharge process of Si/cross-linked PEI anode and cycling stability of Si anode with different binders. Reproduced with permission from Ref. [190], © Elsevier Ltd. 2019.

additives, and salts are designed to promote Si/SiO$_x$ cyclability, including propylene carbonate (PC), fluoroethylene carbonate (FEC), vinylene carbonate (VC), lithium bis(oxalate)borate (LiBOB), lithium bis(trifluoromethylsulfonyl)imide (LiTFSI), and so forth [203–205].

2.4.1 *Electrolyte additives*

FEC is a representative electrolyte additive that can drastically improve the cycling stability. The primary functions of FEC degradation in stabilizing Si-based anodes are (1) to suppress the reduction of electrolytes because the lowest unoccupied molecular orbital (LUMO) energy of FEC is lower than that of other electrolyte components [201]; (2) to form a stable SEI layer consisting of LiF and –Si–F compounds which do not decompose because of the high bonding energy [206]; and (3) to construct a cross-linked polyether network to inhibit polyethylene oxide (PEO)-type polymeric products formed in the electrolytes [207]. Gasteiger et al. proposed that with the addition of FEC into the electrolyte, the cycling stability of Si-Li half-cells as well as Si-LFP cells was critically improved [208].

Jin et al. reported a new electrolyte additive of mesylethyl-methyl-pyrrolidinium-difluoro(oxalato) borate (MEMP-DFOB) [209]. With the aid of the additive, a dense and stable SEI layer was built on the surface of anode and gas evolution was greatly inhibited at high temperature (Fig. 12(a)). By virtue of MEMP and DFOB functional groups, SiO/Gr anode-based pouch cells showed excellent low and high temperature performances, notably for a high capacity retention of ~ 75% after 900 cycles at 45 °C (Fig. 12(b)). For another example, Inoue et al. combined the non-flammable triethyl-phosphate (TEP)-based electrolyte with FEC additive to increase the safety and energy density of LIBs [210]. They found that the reaction between the electrolyte and the charged anode was significantly reduced because FEC could inhibit the exothermic reaction of the decomposition of TEP. The coin cells with TEP:FEC-based electrolyte realized high capacity retention of ~ 80% after 250 cycles (Fig. 12(c)).

2.4.2 *Novel electrolytes*

It is widely acknowledged that the SEI layer usually originates from the reduction and decomposition of electrolytes on the anode surface. For this reason, the composition of electrolyte has a remarkable influence on the structure and properties of SEI layer. Design and optimization of electrolyte is an effective method to increase the electrochemical performance of silicon-based LIBs. For example, Zheng et al. formulated a non-flammable localized high concentration electrolyte (LHCE) with bis(fluorosulfonyl)imide (LiFSI) salt, dimethoxyethane (DME) solvent, and 2,2,3,3-ttrafluoropropyl ether (HFE) diluent, which leaded preferential anion decomposition. In addition, FEC and lithium DFOB (LiDFOB) were added to form a high-modulus SEI layer enriched in fluorine and boron, effectively shielding the anodes from volume changes [211]. The Si/Li half-cells with FEC and LiDFOB demonstrated a remarkable performance with high ICE of 90.2% compared to that cycled in the carbonate electrolyte. (Fig. 13(a)). Zhang et al. adjusted the solute–solvent structure by the utilization of a new diluent and an optimized electrolyte formulation. A LHCE with 1H,1H,5H-octafluoropentyl-1,1,2,2-tetrafluoroether (OTE) diluent was capable of stably cycling Si anodes at room and high temperatures (60 °C) [194]. OTE-based LHCE inhibited the continuous growth of SEI on the Si anode surface by forming a dense and robust inorganic SEI layer. The mechanical strength of the SEI film was much higher than that of SEI film formed in the traditional electrolyte. Besides, it suppressed the bulk expansion of the Si anode during charge and discharge. With the assistance of OTE diluent, the optimized LHCE exhibited excellent cyclic performance on commercial Si/graphite anodes (Fig. 13(b)).

Recently, ionic liquid (IL) electrolytes have attracted increasing attention because of their high stability, excellent ionic conductivity, low vapor pressures, and wide electrochemical window [212]. Piper et al. designed a Si-room temperature ionic liquid (RTIL) system using cyclized-polyacrylonitrile-based Si nanocomposite (nSi-cPAN) as the anode and pyrrolidinium cation and bis(fluorosulfonyl)imide anion (PYR13FSI) as the electrolyte to construct a highly stable SEI [213]. The 18650 cell with Si-RTIL system achieved average 99.7% CE for the first 100 cycles and 75% capacity retention after 500 cycles. Similarly, Song et al. prepared the $SiO_{1.3}$ film electrode (thickness of 70 nm) through pulsed laser deposition (PLD), and employed 1 M LiTFSI/1-methyl-1-propylpyrrolidinium bis(trifluoromethyl sulfonyl)imide (Py_{13}TFSI) as the IL electrolyte to build a robust and stable SEI layer to suppress the volume expansion of $SiO_{1.3}$ anode during cycles [214]. Therefore, the film electrode showed high CE of 97% with a capacity retention of 88% after 200 cycles.

2.4.3 *Silicon-based solid-state batteries*

Traditional lithium-ion batteries typically use liquid electrolytes consisting of flammable organic solvents that react with active materials to emit volatile gases and may cause fire and explosion.

Table 2 A summary of various polymer binders for Si-based anodes

Binder	Si-based anodes	Binder ratio	1st cycle	Long cycling performance	References
Alg	SiNPs	15%	2,000 mAh·g^{-1} with 94.7% CE at 140 mA·g^{-1}	1,700 mAh·g^{-1} after 100 cycles at 4,200 mA·g^{-1}	[139]
CMC	SiNPs	15%	2,917 mAh·g^{-1} with 62.06% CE at 0.1 C	1,608 mAh·g^{-1} after 50 cycles at 0.1 C	[166]
Renatured DNA/Alg	SiNPs	20%	3,400 mAh·g^{-1} with 84.6% CE at 0.1 C	2,000 mAh·g^{-1} after 160 cycles at 0.5 C	[167]
CMC/GG	SiO_x/graphite	20%	427 mAh·g^{-1} with 73.3% CE	385.7 mAh·g^{-1} after 100 cycles	[165]
KGM	Si@SiO_2	25%	3,731 mAh·g^{-1} with 78.1% CE at 2 A·g^{-1}	1,278 mAh·g^{-1} after 1,000 cycles at 2 A·g^{-1}	[215]
PAA	Si@PD	20%	1,927 mAh·g^{-1} with 68.9% CE at 0.1 A·g^{-1}	1,800 mAh·g^{-1} after 100 cycles at 1.5 A·g^{-1}	[216]
Hydrolyzed polyacrylamide	SiNPs	15%	3,000 mAh·g^{-1} with 77% CE at 0.1 C	1,639 mAh·g^{-1} after 100 cycles at C/10	[217]
PVA-g-PAA	SiNPs	10%	3,260.5 mAh·g^{-1} with 82.4% CE at 400 mA·g^{-1}	1,315.8 mAh·g^{-1} after 1,000 cycles at 400 mA·g^{-1}	[218]
PAA-GA	SiNPs	20%	3,739 mAh·g^{-1} with 86.5% CE at 0.05 C	3,028 mAh·g^{-1} after 285 cycles at 0.2 C	[177]
PAA	SiNPs	20%	2,876 mAh·g^{-1} with 82.1% CE at 500 mA·g^{-1}	1,500 mAh·g^{-1} after 500 cycles at 1 A·g^{-1}	[219]
PAA	Si/C	25%	3,088 mAh·g^{-1} with 84.6% CE at 0.1 C	400 mAh·g^{-1} after 100 cycles at C/10	[220]
PANI-PAA	SiNPs	—	2,800 mAh·g^{-1} with 91% CE at 0.2 C	630 mAh·g^{-1} after 800 cycles at 4.2 A·g^{-1}	[175]
PEC/PAA	SiNPs	20%	4,204 mAh·g^{-1} with 84.7% CE at 0.05 C	2,386 mAh·g^{-1} after 100 cycles at 0.2 C	[178]
Polyimide-PEG	SiNPs	20%	3,000 mAh·g^{-1} with 80.5% CE at 0.1 C	2,235.5 mAh·g^{-1} after 200 cycles at 420 mA·g^{-1}	[221]
PMDOPA	SiNPs	20%	3,084 mAh·g^{-1} with 89.6% CE at 0.2 C	1,600 mAh·g^{-1} after 200 cycles at 0.2 C	[222]
GC-g-LiPAA	Si/graphite	10%	745 mAh·g^{-1} with 90.3% CE at 0.1 C	495 mAh·g^{-1} after 100 cycles at 0.1 C	[179]
CS-g-PAANa	SiNPs	30%	2,303 mAh·g^{-1} with 85.96% CE at 420 mA·g^{-1}	1,608 mAh·g^{-1} after 100 cycles at 420 mA·g^{-1}	[180]
CS-g-PANI	SiNPs	20%	4,417 mAh·g^{-1} with 72.4% CE at 1 C	1,087 mAh·g^{-1} after 200 cycles at 1 C	[223]
CS-g-PAAA	SiNPs	20%	2,550 mAh·g^{-1} with 69% CE at 0.1 C	1,301 mAh·g^{-1} after 300 cycles at 4.2 A·g^{-1}	[224]
TA-PAA	SiSMPs	10%	3,012 mAh·g^{-1} with 90% CE at 0.1 A·g^{-1}	2,002 mAh·g^{-1} after 100 cycles at 0.6 A·g^{-1}	[187]
Hyperbranched PEI	SiNPs	20%	3,300 mAh·g^{-1} with 91.6% CE at 500 mA·g^{-1}	2,180 mAh·g^{-1} after 100 cycles at 500 mA·g^{-1}	[190]
PU elastomer	SiNPs	20%	3,400 mAh·g^{-1} with 85% CE at 0.2 C	2,414 mAh·g^{-1} after 100 cycles at 0.2 C	[225]
Crosslinked SA-PAA	SiNPs	10%	2,471 mAh·g^{-1} with 86.9% CE at 200 mA·g^{-1}	945 mAh·g^{-1} after 110 cycles at 200 mA·g^{-1}	[191]
PEDOT:PSS	SiNPs	27%	2,855.7 mAh·g^{-1} with 85.6% CE at 500 mA·g^{-1}	1,951.5 mAh·g^{-1} after 200 cycles at 500 mA·g^{-1}	[226]
c-PAM	SiNPs	15%	3,224.5 mAh·g^{-1} with 86.9% CE at 0.1 C	2,843 mAh·g^{-1} after 100 cycles at 0.1 C	[188]
ppSA-ppCMC	SiNPs	10%	3,881 mAh·g^{-1} with 82.6% CE at 50 mA·g^{-1}	1,863 mAh·g^{-1} after 150 cycles at 500 mA·g^{-1}	[183]
c-PAA-DS	Void@SiO_x@C	10%	751 mAh·g^{-1} with 61.3% CE at 100 mA·g^{-1}	696 mAh·g^{-1} after 500 cycles at 500 mA·g^{-1}	[184]
Sn^{4+}-c-PEDOT:PSS	SiNPs	20%	3,400 mAh·g^{-1} with 80% CE at 1 A·g^{-1}	1,876.4 mAh·g^{-1} after 100 cycles at 1 A·g^{-1}	[227]
PF-COONa	SiNPs	33.3%	4,396 mAh·g^{-1} with 68.4% CE at 420 mA·g^{-1}	2,806 mAh·g^{-1} after 100 cycles at 420 mA·g^{-1}	[228]
c-CMC-CPAM	SiNPs	20%	3,460.9 mAh·g^{-1} with 92% CE at 0.1 C	1,906.4 mAh·g^{-1} after 100 cycles at 300 mA·g^{-1}	[229]
Pyrene-based (PPyMAA)	SiNPs	10%	3,928.8 mAh·g^{-1} with 82.08% CE at 420 mA·g^{-1}	2,200 mAh·g^{-1} after 180 cycles at 420 mA·g^{-1}	[230]
Slide-ring PR-PAA	SiMPs	10%	2,971 mAh·g^{-1} with 91.22% CE at 100 mA·g^{-1}	2.43 mAh·cm^{-2} after 150 cycles at 0.64 mA·cm^{-2}	[231]
C-chitosan	SiNPs	8%	4,270 mAh·g^{-1} with 89% CE at 200 mA·g^{-1}	766 mAh·g^{-1} after 100 cycles at 200 mA·g^{-1}	[140]
Guar gum	SiNPs	5%	1,250 mAh·g^{-1} with 95% CE at 3,600 mA·g^{-1}	1,000 mAh·g^{-1} after 100 cycles at 3600 mA·g^{-1}	[232]
Crosslinked CMC-PEG	SiNPs	10%	3,816.6 mAh·g^{-1} with 81% CE at 357.2 mA·g^{-1}	2,000 mAh·g^{-1} after 350 cycles at 0.5 C	[233]
Boronic crosslinked guar	SiNPs	10%	2,750 mAh·g^{-1} with 82.7% CE at 0.05 C	2,400 mAh·g^{-1} after 100 cycles at 0.2 C	[234]
PAA-PEGPBI	SiNPs	10%	2,400 mAh·g^{-1} with 79.8% CE at 1,000 mA·g^{-1}	1,221 mAh·g^{-1} after 50 cycles at 1,000 mA·g^{-1}	[235]
PFP-g-PEG	SiNPs	10%	2,625 mAh·g^{-1} with 72% CE at 0.1 C	605 mAh·g^{-1} after 1,000 cycles at C/3	[236]
PPyMADMA	Si-alloy	10%	845.2 mAh·g^{-1} with 64.64% CE at 0.1 C	800 mAh·g^{-1} after 100 cycles at 0.1 C	[237]
CG	SiNPs	10%	3,788 mAh·g^{-1} with 80% CE at 0.2 C	1,500 mAh·g^{-1} after 700 cycles at 840 mA·g^{-1}	[238]

Due to the impressive advantages such as high safety and energy density, solid state batteries have emerged as promising energy storages for realizing advanced LIBs. It should be noted that the formation of SEI layer only occurs at contact surface areas between adjacent particles [239].

In silicon-based solid-state batteries, the solid electrolyte (SE) provides a rapid diffusion channel for Li^+ and serves as a battery membrane. Nevertheless, poor contact between the solid electrolyte and the electrode results in poor conductivity and high resistance [240]. The performance of silicon-based solid-state

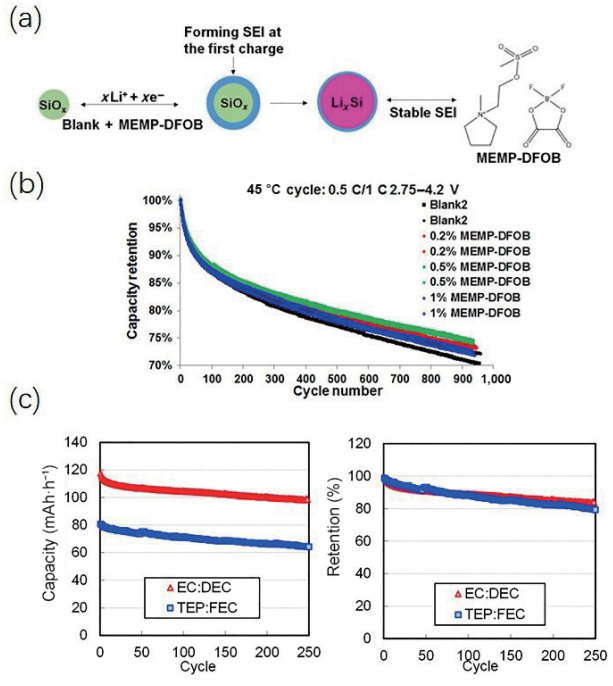

Figure 12 Electrolyte additives for silicon-based LIBs. (a) The illustration of SEI formation; and (b) long-term cycling stability of SiO/Gr||NCA pouch cells (NCA: $LiNi_{0.8}Co_{0.15}Al_{0.05}O_2$) with different contents of MEMP-DFOB at 45 °C. Reproduced with permission from Ref. [209], © Elsevier B.V. 2021. (c) Cycling performance with EC:DEC (EC: ethylene carbonate, DEC: diethyle carbonate) or TEP:FEC-based electrolyte. Reproduced with permission from Ref. [210], © Elsevier B.V. 2014.

batteries can be improved by increasing the contact area by combining solid electrolyte and anode material as the composite electrode [241–244]. For example, Okuno and his coworkers presented that nanoporous Si particles were prepared by using Mg_2Si to facilitate the reduction of SiO_2 fumes and composited with Li_3PS_4 solid electrolyte as the anode material to adapt the volume expansion of Si particles [245]. Nanoporous Si was in full contact with the electrolyte, giving rise to low interfacial resistance and increased cycling stability. Paik et al. constructed Si nanoparticles composited with CNF coated with Li_6PS_5Cl (LPSCl) (Si/CNF@LPSCl) as the anode for all-solid-state batteries [246]. Coating solid electrolyte on the Si/CNF surface could increase the contact area between the anode and solid electrolyte to boost the Li^+ diffusion, leading to the enhancement of electrochemical performance. The Si/CNF@LPSCl anode showed a high discharge capacity of 1172 mAh·g^{-1} at 0.1 C with a capacity retention of 84% after 50 cycles (Fig. 14(a)). On the other hand, quasi-solid-state batteries also hold great promise for becoming the next generation of battery because they can significantly increase the contact area between electrodes and electrolytes. A quasi-solid-state battery was reported by Wang et al. in terms of redox chemistry between a Li_2S cathode and hollow Si anode in gel polymer electrolyte (GPE) [247]. The hollow CoN nanoshell (h-CoN) of cathode decreased the reaction barrier between the adsorption of lithium polysulfides and redox conversion, improving the catalytic activity and boosting the redox kinetics. The quasi-solid-state Li_2S||Si battery exhibited a high energy of 802 Wh·kg^{-1} with a long cyclic life at extreme temperatures (from −20 to 60 °C) (Fig. 14(b)).

3 Summary and outlook

In summary, Si and SiO_x have been considered as potential anodes for next-generation state-of-the-art advanced LIBs because of their high theoretical capacities, low costs, and reasonable redox potentials. Although Si and SiO_x have excellent properties compared to other praised anode materials, there are still some main challenges we cannot bypass, namely massive volume expansion of Si-based anodes, unstable growth of SEI, low initial Coulombic efficiency, and security issues. From this perspective, we present the major challenges and recent developments in the modification strategies of Si-based anodes. Despite these efforts, progresses in commercial application of silicon-based lithium-ion batteries are still limited by the short cycle life (generally less than 200 cycles). To address these challenges, the following aspects need to be considered.

First, priority should be given to the rational design and synthesis of nanocrystalline Si-based materials to tackle the issue of huge volume variation of Si or SiO_x particles upon

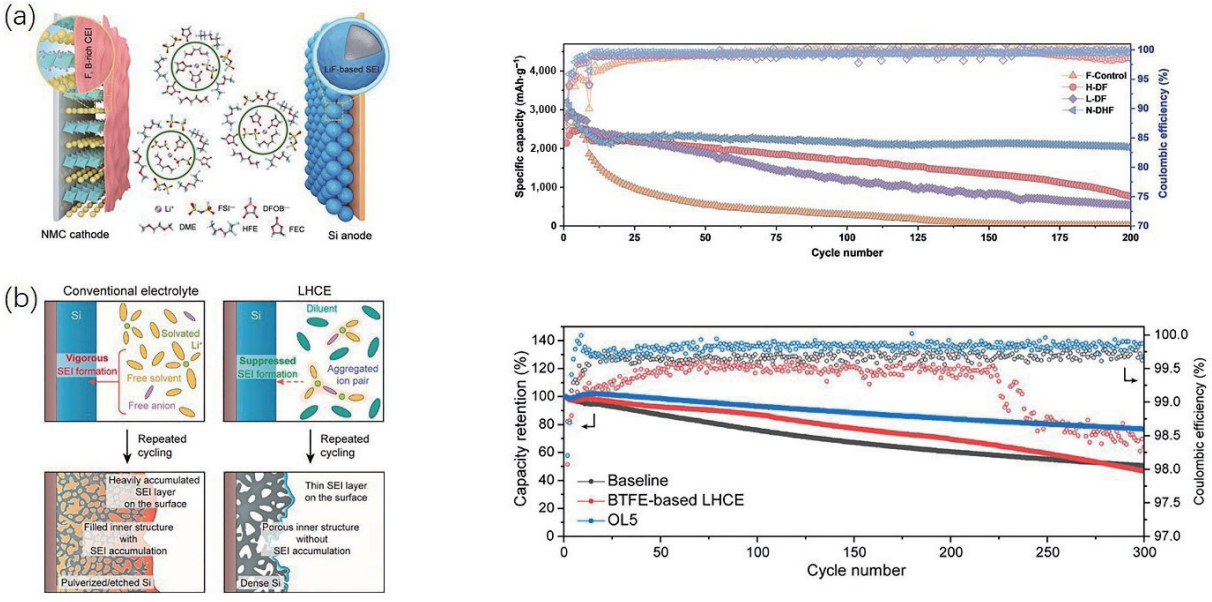

Figure 13 Novel electrolytes for silicon-based LIBs. (a) Scheme of the NMC532/Si battery configuration with the nonflammable N-DHF electrolyte (1.2 M LiFSI/0.05 M LiDFOB in DME/HFE/FEC (3:6:1 by volume)); long-term cycling performance and CE of the Si anode at 0.2 C after pre-cycling under 0.05 and 0.1 C for three and five cycles, respectively. 1 C = 4.2 A·g^{-1}. Reproduced with permission from Ref. [211], © Wiley-VCH GmbH 2021. (b) Influence of the baseline (conventional carbonate electrolyte) and OL (OTE-based localized high-concentration electrolytes) electrolytes on the degradation of Si anodes, and the long-term cycling performance and CE of Si/graphite NMC532 full cells with different electrolytes at 45 °C. Reproduced with permission from Ref. [194], © American Chemical Society 2021.

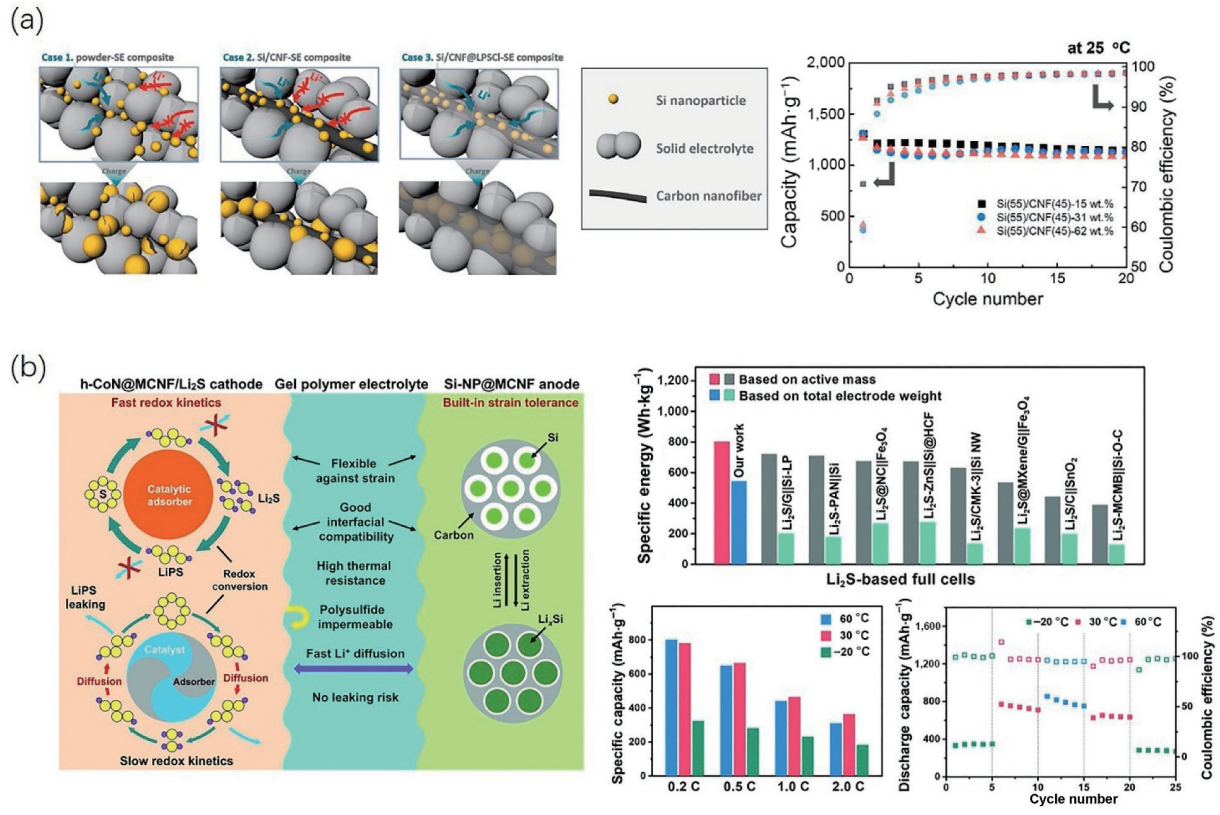

Figure 14 Solid-state electrolytes for silicon-based LIBs. (a) Schematic illustration of the active material and solid electrolyte composite electrode (case 1) Si particle-SE composite, (case 2) Si/CNF-SE composite, and (case 3) Si/CNF@LPSCl-SE composite. Reproduced with permission from Ref. [246], © Elsevier B.V. 2021. (b) Schematic illustration of the configuration and merits of quasi-solid-state h-CoN@MCNF/Li_2S||Si-NP@MCNF full cells; comparison with the reported Li_2S-based full cells in specific energy; capacity retention at various current rates; and discharge capacities against continuously varied operating temperature at 0.2 C. Reproduced with permission from Ref. [247], © The Royal Society of Chemistry 2021.

charge/discharge processes. Undoubtedly, the main trends of Si-based materials are forward to nano-scale and composite structure to minimize volume expansion while improving the electrical conductivity. The nanostructure of Si-based composites not only provides great mechanical strength but boosts the electrochemical performance. However, it is important to note that porous nanostructures with high specific surface areas will permanently consume excessive amounts of electrolyte and Li^+ during the initial cycle process to form the SEI layer, leading to low ICE, irreversible capacity loss, and low energy density. Meanwhile, surface coating as an effective method can enhance the conductivity as well as increase ICE of Si-based anodes, but a lot of active sites are buried by the coated layer and inevitably irreversible capacity loss can be observed. On the other hand, till date Si or SiO_x nanostructures have not been synthesized in an economical way, such as "top down" strategies including high energy mechanical milling and high temperature thermal reduction and "bottom up" strategies including chemical vapor deposition and classical vapor–liquid–solid growth [36]. It is currently very laborious and complicated and not suitable for practical application. Therefore, in pursuit of high-performance Si-based LIBs, vigorously developing efficient and low manufacturing cost of preparation technologies of Si-based composite electrodes is indispensable. Nowadays, the tap density of practical silicon anode-based lithium-ion batteries is generally less than 0.3 $g{\cdot}cm^{-3}$ [248]. Such a low tap density often results in the actual volume capacity for the anode being far less than the theoretical volume capacity of Si or SiO_x. On the other hand, low Si mass loading can extend the battery lifespan, but it will also lead to the reduction of the specific capacity of the electrode. Hence, for real-world applications, we need to take all these factors into consideration to weigh all the pros and cons to achieve high-performance LIBs with Si-based anodes.

Second, the ICE of bare Si or SiO_x is typically less than 80%, which means that a large amount of active lithium is lost during the lithiation of silicon or silicon oxides. Prelithiation methods bring a ray of hope to Si-based rechargeable batteries because prelithiation can compensate the irreversible lithium loss attributed to the formation of SEI layer during the initial charge–discharge process. Up to now, various prelithiation approaches have been reported, including physical blending, chemical prelithiation, and electrochemical prelithiation [249]. However, large-scale industrial application has not yet been realized owing to their respective drawbacks. Developing low cost, simple operation, and controllable degree of prelithiation technologies is of great significance to improve the ICE of Si-based anodes. It is crucial that the ICE of more than 90% is necessary for practical conditions.

Third, reversible Coulombic efficiency as another key issue should be taken into consideration seriously for large-scale commercial application. Both electrolyte additives and binders play crucial roles for the reversible Coulombic efficiency and the performance of batteries. Design of novel solvents and additives with excellent ion transport and large potential window along with binders with good mechanical properties to achieve better battery performance is necessary. Meanwhile, the utilization of solid electrolyte is one of the effective ways to solve safety issues. It is noteworthy that the progress of constructing Si-based all solid-state battery is held back by its high production cost and large interface impedance between solid electrolyte and electrode [239].

Forth, we need to holistically understand the formation, composition, morphology, and evolution of SEI layer via advanced and/or *in-situ* characterization technologies, such as atomic force

microscopy (AFM), *in-situ* X-ray photoelectron spectroscopy (XPS), cryogenic transmission electron microscopy (cryo-TEM), and secondary ion mass spectrometry (SIMS). Combined with first-principles calculations, SEI structure and corresponding dynamic evolution will be distinctly revealed. The SEI components are strongly affected by the solvent, additive, and electrode material. Since the main composition of the SEI layer varies from electrolyte to electrolyte, it is essential to figure out the keys of SEI film impacting on the cycling performance of Si-based anode. In other words, it is of extremely vital significance for us to further optimize the structure of electrode materials and the composition of electrolytes.

Acknowledgements

This work was supported by the National Natural Science Foundation of China (Nos. 52122209, 52111530050, and 51772147), Postgraduate Research & Practice Innovation Program of Jiangsu Province (No. SJCX22_0433), and the Research Foundation of State Key Lab (Nos. ZK201906 and ZK201805).

References

[1] Winter, M.; Besenhard, J. O.; Spahr, M. E.; Novák, P. Insertion electrode materials for rechargeable lithium batteries. *Adv. Mater.* **1998**, *10*, 725–763.

[2] Choi, J. W.; Aurbach, D. Promise and reality of post-lithium-ion batteries with high energy densities. *Nat. Rev. Mater.* **2016**, *1*, 16013.

[3] Dunn, B.; Kamath, H.; Tarascon, J. M. Electrical energy storage for the grid: A battery of choices. *Science* **2011**, *334*, 928–935.

[4] Chae, S.; Park, S.; Ahn, K.; Nam, G.; Lee, T.; Sung, J.; Kim, N.; Cho, J. Gas phase synthesis of amorphous silicon nitride nanoparticles for high-energy LIBs. *Energy Environ. Sci.* **2020**, *13*, 1212–1221.

[5] Ryu, J.; Hong, D.; Lee, H. W.; Park, S. Practical considerations of Si-based anodes for lithium-ion battery applications. *Nano Res.* **2017**, *10*, 3970–4002.

[6] Zhang, H. M.; Zhao, S. W.; Huang, F. Q. A comparative overview of carbon anodes for nonaqueous alkali metal-ion batteries. *J. Mater. Chem. A* **2021**, *9*, 27140–27169.

[7] Chae, S.; Choi, S. H.; Kim, N.; Sung, J.; Cho, J. Integration of graphite and silicon anodes for the commercialization of high-energy lithium-ion batteries. *Angew. Chem., Int. Ed.* **2020**, *59*, 110–135.

[8] Xu, K. Nonaqueous liquid electrolytes for lithium-based rechargeable batteries. *Chem. Rev.* **2004**, *104*, 4303–4418.

[9] Szczech, J. R.; Jin, S. Nanostructured silicon for high capacity lithium battery anodes. *Energy Environ. Sci.* **2011**, *4*, 56–72.

[10] Reddy, M. V.; Rao, G. V. S.; Chowdari, B. V. R. Metal oxides and oxysalts as anode materials for Li ion batteries. *Chem. Rev.* **2013**, *113*, 5364–5457.

[11] Xu, W.; Wang, J. L.; Ding, F.; Chen, X. L.; Nasybutin, E.; Zhang, Y. H.; Zhang, J. G. Lithium metal anodes for rechargeable batteries. *Energy Environ. Sci.* **2014**, *7*, 513–537.

[12] Tarascon, J. M.; Armand, M. Issues and challenges facing rechargeable lithium batteries. *Nature* **2001**, *414*, 359–367.

[13] Lin, D. C.; Liu, Y. Y.; Cui, Y. Reviving the lithium metal anode for high-energy batteries. *Nat. Nanotechnol.* **2017**, *12*, 194–206.

[14] Su, X.; Wu, Q. L.; Li, J. C.; Xiao, X. C.; Lott, A.; Lu, W. Q.; Sheldon, B. W.; Wu, J. Silicon-based nanomaterials for lithium-ion batteries: A review. *Adv. Energy Mater.* **2014**, *4*, 1300882.

[15] McDowell, M. T.; Lee, S. W.; Nix, W. D.; Cui, Y. 25th anniversary article: Understanding the lithiation of silicon and other alloying anodes for lithium-ion batteries. *Adv. Mater.* **2013**, *25*, 4966–4985.

[16] Son, Y.; Sim, S.; Ma, H.; Choi, M.; Son, Y.; Park, N.; Cho, J.; Park, M. Exploring critical factors affecting strain distribution in 1D silicon-based nanostructures for lithium-ion battery anodes. *Adv. Mater.* **2018**, *30*, 1705430.

[17] Ge, M.; Fang, X.; Rong, J.; Zhou, C. Review of porous silicon preparation and its application for lithium-ion battery anodes. *Nanotechnology* **2013**, *24*, 422001.

[18] Shen, X. H.; Tian, Z. Y.; Fan, R. J.; Shao, L.; Zhang, D. P.; Cao, G. L.; Kou, L.; Bai, Y. Z. Research progress on silicon/carbon composite anode materials for lithium-ion battery. *J. Energy Chem.* **2018**, *27*, 1067–1090.

[19] Lee, J. K.; Oh, C.; Kim, N.; Hwang, J. Y.; Sun, Y. K. Rational design of silicon-based composites for high-energy storage devices. *J. Mater. Chem. A* **2016**, *4*, 5366–5384.

[20] Bommier, C.; Ji, X. L. Electrolytes, SEI formation, and binders: A review of nonelectrode factors for sodium-ion battery anodes. *Small* **2018**, *14*, e1703576.

[21] Wu, H.; Cui, Y. Designing nanostructured Si anodes for high energy lithium ion batteries. *Nano Today* **2012**, *7*, 414–429.

[22] Zhou, Y.; Guo, H. J.; Wang, Z. X.; Li, X. H.; Zhou, R.; Peng, W. J. Improved electrochemical performance of Si/C material based on the interface stability. *J. Alloys Compd.* **2017**, *725*, 1304–1312.

[23] Li, T.; Yang, J. Y.; Lu, S. G.; Wang, H.; Ding, H. Y. Failure mechanism of bulk silicon anode electrodes for lithium-ion batteries. *Rare Met.* **2013**, *32*, 299–304.

[24] Yoon, T.; Nguyen, C. C.; Seo, D. M.; Lucht, B. L. Capacity fading mechanisms of silicon nanoparticle negative electrodes for lithium ion batteries. *J. Electrochem. Soc.* **2015**, *162*, A2325–A2330.

[25] Yuda, A. P.; Koraag, P. Y. E.; Iskandar, F.; Wasisto, H. S.; Sumboja, A. Advances of the top-down synthesis approach for high-performance silicon anodes in Li-ion batteries. *J. Mater. Chem. A* **2021**, *9*, 18906–18926.

[26] Liang, B.; Liu, Y. P.; Xu, Y. H. Silicon-based materials as high capacity anodes for next generation lithium ion batteries. *J. Power Sources* **2014**, *267*, 469–490.

[27] Salah, M.; Hall, C.; Murphy, P.; Francis, C.; Kerr, R.; Stoehr, B.; Rudd, S.; Fabretto, M. Doped and reactive silicon thin film anodes for lithium ion batteries: A review. *J. Power Sources* **2021**, *506*, 230194.

[28] Shen, T.; Yao, Z. J.; Xia, X. H.; Wang, X. L.; Gu, C. D.; Tu, J. P. Rationally designed silicon nanostructures as anode material for lithium-ion batteries. *Adv. Eng. Mater.* **2018**, *20*, 1700591.

[29] Kwon, T. W.; Choi, J. W.; Coskun, A. The emerging era of supramolecular polymeric binders in silicon anodes. *Chem. Soc. Rev.* **2018**, *47*, 2145–2164.

[30] Feng, K.; Li, M.; Liu, W. W.; Kashkooli, A. G.; Xiao, X. C.; Cai, M.; Chen, Z. W. Silicon-based anodes for lithium-ion batteries: From fundamentals to practical applications. *Small* **2018**, *14*, 1702737.

[31] Thackeray, M. M.; Wolverton, C.; Isaacs, E. D. Electrical energy storage for transportation-approaching the limits of, and going beyond, lithium-ion batteries. *Energy Environ. Sci.* **2012**, *5*, 7854–7863.

[32] Schiele, A.; Breitung, B.; Hatsukade, T.; Berkes, B. B.; Hartmann, P.; Janek, J.; Brezesinski, T. The critical role of fluoroethylene carbonate in the gassing of silicon anodes for lithium-ion batteries. *ACS Energy Lett.* **2017**, *2*, 2228–2233.

[33] Casimir, A.; Zhang, H. G.; Ogoke, O.; Amine, J. C.; Lu, J.; Wu, G. Silicon-based anodes for lithium-ion batteries: Effectiveness of materials synthesis and electrode preparation. *Nano Energy* **2016**, *27*, 359–376.

[34] Zuo, X. X.; Zhu, J.; Müller-Buschbaum, P.; Cheng, Y. J. Silicon based lithium-ion battery anodes: A chronicle perspective review. *Nano Energy* **2017**, *31*, 113–143.

[35] Tao, W.; Wang, P.; You, Y.; Park, K.; Wang, C. Y.; Li, Y. K.; Cao, F. F.; Xin, S. Strategies for improving the storage performance of silicon-based anodes in lithium-ion batteries. *Nano Res.* **2019**, *12*, 1739–1749.

[36] Li, P.; Zhao, G. Q.; Zheng, X. B.; Xu, X.; Yao, C. H.; Sun, W. P.; Dou, S. X. Recent progress on silicon-based anode materials for practical lithium-ion battery applications. *Energy Storage Mater.* **2018**, *15*, 422–446.

[37] Yang, Y.; Yuan, W.; Kang, W. Q.; Ye, Y. T.; Yuan, Y. H.; Qiu, Z. Q.; Wang, C.; Zhang, X. Q.; Ke, Y. Z.; Tang, Y. Silicon-nanoparticle-based composites for advanced lithium-ion battery anodes. *Nanoscale* **2020**, *12*, 7461–7484.

[38] Zafar Abbas Manj, R.; Zhang, F. Z.; Ur Rehman, W.; Luo, W.; Yang, J. P. Toward understanding the interaction within silicon-based anodes for stable lithium storage. *Chem. Eng. J.* **2020**, *385*, 123821.

[39] Basu, S.; Suresh, S.; Ghatak, K.; Bartolucci, S. F.; Gupta, T.; Hundekar, P.; Kumar, R.; Lu, T. M.; Datta, D.; Shi, Y. F. et al. Utilizing van der Waals slippery interfaces to enhance the electrochemical stability of silicon film anodes in lithium-ion batteries. *ACS Appl. Mater. Interfaces* **2018**, *10*, 13442–13451.

[40] Chen, Q. L.; Zheng, H. F.; Yang, Y. F.; Xie, Q. S.; Ma, Y. T.; Wang, L. S.; Peng, D. L. Ion- and electron-conductive buffering layer-modified Si film for use as a high-rate long-term lithium-ion battery anode. *ChemSusChem* **2019**, *12*, 252–260.

[41] Liu, J. J.; Yang, Y.; Lyu, P.; Nachtigall, P.; Xu, Y. X. Few-layer silicene nanosheets with superior lithium-storage properties. *Adv. Mater.* **2018**, *30*, e1800838.

[42] Sadeghipari, M.; Mohajerzadeh, M. A.; Hajmirzaheydarali, M.; Mashayekhi, A.; Mohajerzadeh, S. A novel approach to realize Si-based porous wire-in-tube nanostructures for high-performance lithium-ion batteries. *Small* **2018**, *14*, e1800615.

[43] Schmerling, M.; Fenske, D.; Peters, F.; Schwenzel, J.; Busse, M. Lithiation behavior of silicon nanowire anodes for lithium-ion batteries: Impact of functionalization and porosity. *ChemPhysChem* **2018**, *19*, 123–129.

[44] Xu, S.; Fan, X. F.; Liu, J. L.; Singh, D. J.; Jiang, Q.; Zheng, W. T. Adsorption of Li on single-layer silicene for anodes of Li-ion batteries. *Phys. Chem. Chem. Phys.* **2018**, *20*, 8887–8896.

[45] Xu, T.; Wang, D.; Qiu, P.; Zhang, J.; Wang, Q.; Xia, B. J.; Xie, X. H. *In situ* synthesis of porous Si dispersed in carbon nanotube intertwined expanded graphite for high-energy lithium-ion batteries. *Nanoscale* **2018**, *10*, 16638–16644.

[46] Liu, Y. X.; Qin, L. J.; Liu, F.; Fan, Y. M.; Ruan, J. J.; Zhang, S. J. Interpenetrated 3D porous silicon as high stable anode material for Li-Ion battery. *J. Power Sources* **2018**, *406*, 167–175.

[47] Liu, X. H.; Zhong, L.; Huang, S.; Mao, S. X.; Zhu, T.; Huang, J. Y. Size-dependent fracture of silicon nanoparticles during lithiation. *ACS Nano* **2012**, *6*, 1522–1531.

[48] Kim, H.; Seo, M.; Park, M. H.; Cho, J. A critical size of silicon nano-anodes for lithium rechargeable batteries. *Angew. Chem., Int. Ed.* **2010**, *49*, 2146–2149.

[49] Yu, B. C.; Hwa, Y.; Park, C. M.; Sohn, H. J. Reaction mechanism and enhancement of cyclability of SiO anodes by surface etching with NaOH for Li-ion batteries. *J. Mater. Chem. A* **2013**, *1*, 4820–4825.

[50] Song, H. C.; Wang, S.; Song, X. Y.; Yang, H. F.; Du, G. H.; Yu, L. W.; Xu, J.; He, P.; Zhou, H. S.; Chen, K. J. A bottom-up synthetic hierarchical buffer structure of copper silicon nanowire hybrids as ultra-stable and high-rate lithium-ion battery anodes. *J. Mater. Chem. A* **2018**, *6*, 7877–7886.

[51] Li, Z. H.; He, Q.; He, L.; Hu, P.; Li, W.; Yan, H. W.; Peng, X. Z.; Huang, C. Y.; Mai, L. Q. Self-sacrificed synthesis of carbon-coated SiO_x nanowires for high capacity lithium ion battery anodes. *J. Mater. Chem. A* **2017**, *5*, 4183–4189.

[52] Li, H. D.; Li, H. Y.; Lai, Y. Z.; Yang, Z. W.; Yang, Q.; Liu, Y.; Zheng, Z.; Liu, Y. X.; Sun, Y.; Zhong, B. H. et al. Revisiting the preparation progress of nano-structured Si anodes toward industrial application from the perspective of cost and scalability. *Adv. Energy Mater.* **2022**, *12*, 2102181.

[53] Meng, X.; Sasaki, K.; Sano, K.; Yuan, P. L.; Tatsuoka, H. Synthesis of crystalline Si-based nanosheets by extraction of Ca from $CaSi_2$ in inositol hexakisphosphate solution. *Jpn. J. Appl. Phys.* **2017**, *56*, 05DE02.

[54] Wang, X. H.; Sun, L. M.; Hu, X. N.; Susantyoko, R. A.; Zhang, Q. Ni-Si nanosheet network as high performance anode for Li ion batteries. *J. Power Sources* **2015**, *280*, 393–396.

[55] Zhang, L.; Deng, J. W.; Liu, L. F.; Si, W. P.; Oswald, S.; Xi, L. X.; Kundu, M.; Ma, G. Z.; Gemming, T.; Baunack, S. et al. Hierarchically designed SiO_x/SiO_y bilayer nanomembranes as stable anodes for lithium ion batteries. *Adv. Mater.* **2014**, *26*, 4527–4532.

[56] Sämann, C.; Kelesiadou, K.; Hosseinioun, S. S.; Wachtler, M.; Köhler, J. R.; Birke, K. P.; Schubert, M. B.; Werner, J. H. Laser porosificated silicon anodes for lithium ion batteries. *Adv. Energy Mater.* **2018**, *8*, 1701705.

[57] Zhang, X. H.; Qiu, X. Y.; Kong, D. B.; Zhou, L.; Li, Z. H.; Li, X. L.; Zhi, L. J. Silicene flowers: A dual stabilized silicon building block for high-performance lithium battery anodes. *ACS Nano* **2017**, *11*, 7476–7484.

[58] Chen, M.; Jing, Q. S.; Sun, H. B.; Xu, J. Q.; Yuan, Z. Y.; Ren, J. T.; Ding, A. X.; Huang, Z. Y.; Dong, M. Y. Engineering the core–shell-structured NCNTs-Ni_2Si@porous Si composite with robust Ni–Si interfacial bonding for high-performance Li-ion batteries. *Langmuir* **2019**, *35*, 6321–6332.

[59] Gao, P. B.; Huang, X.; Zhao, Y. T.; Hu, X. D.; Cen, D. C.; Gao, G. H.; Bao, Z. H.; Mei, Y. F.; Di, Z. F.; Wu, G. M. Formation of Si hollow structures as promising anode materials through reduction of silica in $AlCl_3$-NaCl molten salt. *ACS Nano* **2018**, *12*, 11481–11490.

[60] Yu, B. C.; Hwa, Y.; Kim, J. H.; Sohn, H. J. A new approach to synthesis of porous SiO_x anode for Li-ion batteries via chemical etching of Si crystallites. *Electrochim. Acta* **2014**, *117*, 426–430.

[61] Yang, L. Y.; Li, S. T.; Wang, S. Y.; Zhu, K. J.; Liu, J.; Chen, Y. W.; Tang, S. S.; Mi, H. Y.; Chen, F. J. A unique intricate hollow Si nanocomposite designed for lithium storage. *J. Alloys Compd.* **2018**, *758*, 177–183.

[62] Jiang, T.; Zhang, S. C.; Qiu, X. P.; Zhu, W. T.; Chen, L. Q. Preparation and characterization of silicon-based three-dimensional cellular anode for lithium ion battery. *Electrochem. Commun.* **2007**, *9*, 930–934.

[63] Nguyen, C. C.; Song, S. W. Interfacial structural stabilization on amorphous silicon anode for improved cycling performance in lithium-ion batteries. *Electrochim. Acta* **2010**, *55*, 3026–3033.

[64] Bao, Q.; Lee, J.; Duh, J. G. Building 3D porous, elastic and hydrophilic current collectors: Prolonging the cycling life of Si based anode for lithium ion batteries. *Mater. Lett.* **2017**, *202*, 28–31.

[65] Fu, K.; Yildiz, O.; Bhanushali, H.; Wang, Y. X.; Stano, K.; Xue, L. G.; Zhang, X. W.; Bradford, P. D. Aligned carbon nanotube-silicon sheets: A novel nano-architecture for flexible lithium ion battery electrodes. *Adv. Mater.* **2013**, *25*, 5109–5114.

[66] Kim, S. W.; Yun, J. H.; Son, B.; Lee, Y. G.; Kim, K. M.; Lee, Y. M.; Cho, K. Y. Graphite/silicon hybrid electrodes using a 3D current collector for flexible batteries. *Adv. Mater.* **2014**, *26*, 2977–2982.

[67] Liu, Z. J.; Bai, S.; Liu, B. L.; Guo, P. Q.; Lv, M. Z.; Liu, D. Q.; He, D. Y. Interfacial modification of a lightweight carbon foam current collector for high-energy density Si/LCO lithium-ion batteries. *J. Mater. Chem. A* **2017**, *5*, 13168–13175.

[68] Zhang, W.; Zuo, P. J.; Chen, C.; Ma, Y. L.; Cheng, X. Q.; Du, C. Y.; Gao, Y. Z.; Yin, G. P. Facile synthesis of binder-free reduced graphene oxide/silicon anode for high-performance lithium ion batteries. *J. Power Sources* **2016**, *312*, 216–222.

[69] Wang, J.; Zhou, M. J.; Tan, G. Q.; Chen, S.; Wu, F.; Lu, J.; Amine, K. Encapsulating micro-nano Si/SiO_x into conjugated nitrogen-doped carbon as binder-free monolithic anodes for advanced lithium ion batteries. *Nanoscale* **2015**, *7*, 8023–8034.

[70] Zhao, T. T.; Zhu, D. L.; Li, W. R.; Li, A. J.; Zhang, J. J. Novel design and synthesis of carbon-coated porous silicon particles as high-performance lithium-ion battery anodes. *J. Power Sources* **2019**, *439*, 227027.

[71] Polat, B. D.; Keles, O. The effect of copper coating on nanocolumnar silicon anodes for lithium ion batteries. *Thin Solid Films* **2015**, *589*, 543–550.

[72] Chen, J. J.; Lu, X. Y.; Sun, J.; Xu, F. F. Si@C nanosponges application for lithium ions batteries synthesized by templated

magnesiothermic route. *Mater. Lett.* **2015**, *152*, 256–259.
[73] Sourice, J.; Quinsac, A.; Leconte, Y.; Sublemontier, O.; Porcher, W.; Haon, C.; Bordes, A.; De Vito, E.; Boulineau, A.; Larbi, S. J. S. et al. One-step synthesis of Si@C nanoparticles by laser pyrolysis: High-capacity anode material for lithium-ion batteries. *ACS Appl. Mater. Interfaces* **2015**, *7*, 6637–6644.
[74] Li, W. Y.; Tang, Y. B.; Kang, W. P.; Zhang, Z. Y.; Yang, X.; Zhu, Y.; Zhang, W. J.; Lee, C. S. Core–shell Si/C nanospheres embedded in bubble sheet-like carbon film with enhanced performance as lithium ion battery anodes. *Small* **2015**, *11*, 1345–1351.
[75] Yun, Q. B.; Qin, X. Y.; He, Y. B.; Lv, W.; Kaneti, Y. V.; Li, B. H.; Yang, Q. H.; Kang, F. Y. Micron-sized spherical Si/C hybrids assembled via water/oil system for high-performance lithium ion battery. *Electrochim. Acta* **2016**, *211*, 982–988.
[76] Ensafi, A. A.; Abarghoui, M. M.; Rezaei, B. Metal (Ni and Bi) coated porous silicon nanostructure, high-performance anode materials for lithium ion batteries with high capacity and stability. *J. Alloys Compd.* **2017**, *712*, 233–240.
[77] Gao, A.; Mukherjee, S.; Srivastava, I.; Daly, M.; Singh, C. V. Atomistic origins of ductility enhancement in metal oxide coated silicon nanowires for Li-ion battery anodes. *Adv. Mater. Interfaces* **2017**, *4*, 1700920.
[78] Wang, Y.; Chen, L.; Liu, H. T.; Xiong, Z. M.; Zhao, L.; Liu, S. H.; Huang, C. M.; Zhao, Y. M. Cornlike ordered N-doped carbon coated hollow Fe_3O_4 by magnetic self-assembly for the application of Li-ion battery. *Chem. Eng. J.* **2019**, *356*, 746–755.
[79] Yang, J. P.; Wang, Y. X.; Li, W.; Wang, L. J.; Fan, Y. C.; Jiang, W.; Luo, W.; Wang, Y.; Kong, B.; Selomulya, C. et al. Amorphous TiO_2 shells: A vital elastic buffering layer on silicon nanoparticles for high-performance and safe lithium storage. *Adv. Mater.* **2017**, *29*, 1700523.
[80] Yoon, T.; Bok, T.; Kim, C.; Na, Y.; Park, S.; Kim, K. S. Mesoporous silicon hollow nanocubes derived from metal-organic framework template for advanced lithium-ion battery anode. *ACS Nano* **2017**, *11*, 4808–4815.
[81] Zhang, Q. B.; Chen, H. X.; Luo, L. L.; Zhao, B. T.; Luo, H.; Han, X.; Wang, J. W.; Wang, C. M.; Yang, Y.; Zhu, T. et al. Harnessing the concurrent reaction dynamics in active Si and Ge to achieve high performance lithium-ion batteries. *Energy Environ. Sci.* **2018**, *11*, 669–681.
[82] Kwon, H. T.; Park, A. R.; Lee, S. S.; Cho, H.; Jung, H.; Park, C. M. Nanostructured Si-$FeSi_2$-graphite-C composite: An optimized and practical solution for Si-based anodes for superior Li-ion batteries. *J. Electrochem. Soc.* **2019**, *166*, A2221–A2229.
[83] Wang, S. G.; Wang, T.; Zhong, Y.; Deng, Q. R.; Mao, Y. W.; Wang, G. M. Structure and electrochemical properties of Si-Mn/C core–shell composites for lithium-ion batteries. *JOM* **2020**, *72*, 3037–3045.
[84] Chen, H. D.; He, S. G.; Hou, X. H.; Wang, S. F.; Chen, F. M.; Qin, H. Q.; Xia, Y. C.; Zhou, G. F. Nano-Si/C microsphere with hollow double spherical interlayer and submicron porous structure to enhance performance for lithium-ion battery anode. *Electrochim. Acta* **2019**, *312*, 242–250.
[85] Chen, S. Q.; Shen, L. F.; van Aken, P. A.; Maier, J.; Yu, Y. Dual-functionalized double carbon shells coated silicon nanoparticles for high performance lithium-ion batteries. *Adv. Mater.* **2017**, *29*, 1605650.
[86] Kim, J. M.; Ko, D. J.; Oh, J.; Lee, J.; Hwang, T.; Jeon, Y.; Hooch Antink, W.; Piao, Y. Z. Electrochemically exfoliated graphene as a novel microwave susceptor: The ultrafast microwave-assisted synthesis of carbon-coated silicon-graphene film as a lithium-ion battery anode. *Nanoscale* **2017**, *9*, 15582–15590.
[87] Li, X. L.; Yan, P. F.; Xiao, X. C.; Woo, J. H.; Wang, C. M.; Liu, J.; Zhang, J. G. Design of porous Si/C-graphite electrodes with long cycle stability and controlled swelling. *Energy Environ. Sci.* **2017**, *10*, 1427–1434.
[88] Li, Z. H.; Li, Z. P.; Zhong, W. H.; Li, C. F.; Li, L. Q.; Zhang, H. Y. Facile synthesis of ultrasmall Si particles embedded in carbon framework using Si-carbon integration strategy with superior lithium ion storage performance. *Chem. Eng. J.* **2017**, *319*, 1–8.
[89] Liu, N. T.; Mamat, X.; Jiang, R. Y.; Tong, W.; Huang, Y. D.; Jia, D. Z.; Li, Y. T.; Wang, L.; Wågberg, T.; Hu, G. Z. Facile high-voltage sputtering synthesis of three-dimensional hierarchical porous nitrogen-doped carbon coated Si composite for high performance lithium-ion batteries. *Chem. Eng. J.* **2018**, *343*, 78–85.
[90] Mi, H. W.; Yang, X. D.; Li, Y. L.; Zhang, P. X.; Sun, L. N. A self-sacrifice template strategy to fabricate yolk–shell structured silicon@void@carbon composites for high-performance lithium-ion batteries. *Chem. Eng. J.* **2018**, *351*, 103–109.
[91] Prakash, S.; Zhang, C. F.; Park, J. D.; Razmjooei, F.; Yu, J. S. Silicon core–mesoporous shell carbon spheres as high stability lithium-ion battery anode. *J. Colloid Interface Sci.* **2019**, *534*, 47–54.
[92] Shen, X. D.; Jiang, W. F.; Sun, H. J.; Wang, Y.; Dong, A. G.; Hu, J. H.; Yang, D. Ionic liquid assist to prepare Si@N-doped carbon nanoparticles and its high performance in lithium ion batteries. *J. Alloys Compd.* **2017**, *691*, 178–184.
[93] Shi, J. W.; Gao, H. Y.; Hu, G. X.; Zhang, Q. Core–shell structured Si@C nanocomposite for high-performance Li-ion batteries with a highly viscous gel as precursor. *J. Power Sources* **2019**, *438*, 227001.
[94] Wang, B.; Ryu, J.; Choi, S.; Zhang, X. H.; Pribat, D.; Li, X. L.; Zhi, L. J.; Park, S.; Ruoff, R. S. Ultrafast-charging silicon-based coral-like network anodes for lithium-ion batteries with high energy and power densities. *ACS Nano* **2019**, *13*, 2307–2315.
[95] Xu, Y. H.; Zhu, Y. J.; Han, F. D.; Luo, C.; Wang, C. S. 3D Si/C fiber paper electrodes fabricated using a combined electrospray/electrospinning technique for Li-ion batteries. *Adv. Energy Mater.* **2015**, *5*, 1400753.
[96] Yang, T.; Tian, X. D.; Li, X.; Wang, K.; Liu, Z. J.; Guo, Q. G.; Song, Y. Double core–shell Si@C@SiO_2 for anode material of lithium-ion batteries with excellent cycling stability. *Chem.—Eur. J.* **2017**, *23*, 2165–2170.
[97] Yao, W. Q.; Chen, J.; Zhan, L.; Wang, Y. L.; Yang, S. B. Two-dimensional porous sandwich-like C/Si-graphene-Si/C nanosheets for superior lithium storage. *ACS Appl. Mater. Interfaces* **2017**, *9*, 39371–39379.
[98] Zhang, C. J.; Liang, F. H.; Zhang, W.; Liu, H.; Ge, M. Z.; Zhang, Y. Y.; Dai, J. M.; Wang, H. L.; Xing, G. C.; Lai, Y. K. et al. Constructing mechanochemical durable and self-healing superhydrophobic surfaces. *ACS Omega* **2020**, *5*, 986–994.
[99] Zhang, H. L.; Xu, J. Q.; Zhang, J. J. Preparation and electrochemical properties of core–shelled silicon-carbon composites as anode materials for lithium-ion batteries. *J. Appl. Electrochem.* **2019**, *49*, 1123–1132.
[100] Chen, F. Q.; Han, J. W.; Kong, D. B.; Yuan, Y. F.; Xiao, J.; Wu, S. C.; Tang, D. M.; Deng, Y. Q.; Lv, W.; Lu, J. et al. 1000 $Wh{\cdot}L^{-1}$ lithium-ion batteries enabled by crosslink-shrunk tough carbon encapsulated silicon microparticle anodes. *Natl. Sci. Rev.* **2021**, *8*, nwab012.
[101] Lee, J. I.; Park, S. High-performance porous silicon monoxide anodes synthesized via metal-assisted chemical etching. *Nano Energy* **2013**, *2*, 146–152.
[102] Si, Q.; Hanai, K.; Ichikawa, T.; Phillipps, M. B.; Hirano, A.; Imanishi, N.; Yamamoto, O.; Takeda, Y. Improvement of cyclic behavior of a ball-milled SiO and carbon nanofiber composite anode for lithium-ion batteries. *J. Power Sources* **2011**, *196*, 9774–9779.
[103] Kim, K. W.; Park, H.; Lee, J. G.; Kim, J.; Kim, Y. U.; Ryu, J. H.; Kim, J. J.; Oh, S. M. Capacity variation of carbon-coated silicon monoxide negative electrode for lithium-ion batteries. *Electrochim. Acta* **2013**, *103*, 226–230.
[104] Kobayashi, Y.; Seki, S.; Mita, Y.; Ohno, Y.; Miyashiro, H.; Charest, P.; Guerfi, A.; Zaghib, K. High reversible capacities of graphite and SiO/graphite with solvent-free solid polymer electrolyte for lithium-ion batteries. *J. Power Sources* **2008**, *185*, 542–548.
[105] Lee, D. J.; Ryou, M. H.; Lee, J. N.; Kim, B. G.; Lee, Y. M.; Kim,

H. W.; Kong, B. S.; Park, J. K.; Choi, J. W. Nitrogen-doped carbon coating for a high-performance SiO anode in lithium-ion batteries. *Electrochem. Commun.* **2013**, *34*, 98–101.
[106] Park, C. M.; Choi, W.; Hwa, Y.; Kim, J. H.; Jeong, G.; Sohn, H. J. Characterizations and electrochemical behaviors of disproportionated SiO and its composite for rechargeable Li-ion batteries. *J. Mater. Chem.* **2010**, *20*, 4854–4860.
[107] Xu, S.; Hou, X. D.; Wang, D. N.; Zuin, L.; Zhou, J. G.; Hou, Y.; Mann, M. Insights into the effect of heat treatment and carbon coating on the electrochemical behaviors of SiO anodes for Li-ion batteries. *Adv. Energy Mater.* **2022**, *12*, 2200127.
[108] Park, M.; Lee, D.; Shin, S.; Kim, H. J.; Hyun, J. Flexible conductive nanocellulose combined with silicon nanoparticles and polyaniline. *Carbohydr. Polym.* **2016**, *140*, 43–50.
[109] Li, G.; Huang, L. B.; Yan, M. Y.; Li, J. Y.; Jiang, K. C.; Yin, Y. X.; Xin, S.; Xu, Q.; Guo, Y. G. An integral interface with dynamically stable evolution on micron-sized SiO_x particle anode. *Nano Energy* **2020**, *74*, 104890.
[110] Chen, D. Y.; Mei, X.; Ji, G.; Lu, M. H.; Xie, J. P.; Lu, J. M.; Lee, J. Y. Reversible lithium-ion storage in silver-treated nanoscale hollow porous silicon particles. *Angew. Chem., Int. Ed.* **2012**, *51*, 2409–2413.
[111] Luo, W.; Shen, D. K.; Zhang, R. Y.; Zhang, B. W.; Wang, Y. X.; Dou, S. X.; Liu, H. K.; Yang, J. P. Germanium nanograin decoration on carbon shell: Boosting lithium-storage properties of silicon nanoparticles. *Adv. Funct. Mater.* **2016**, *26*, 7800–7806.
[112] Murugesan, S.; Harris, J. T.; Korgel, B. A.; Stevenson, K. J. Copper-coated amorphous silicon particles as an anode material for lithium-ion batteries. *Chem. Mater.* **2012**, *24*, 1306–1315.
[113] Zhao, Z. Y.; Han, J. W.; Chen, F. Q.; Xiao, J.; Zhao, Y. F.; Zhang, Y. F.; Kong, D. B.; Weng, Z.; Wu, S. C.; Yang, Q. H. Liquid metal remedies silicon microparticulates toward highly stable and superior volumetric lithium storage. *Adv. Energy Mater.* **2022**, *12*, 2103565.
[114] Jeong, G.; Kim, Y. U.; Krachkovskiy, S. A.; Lee, C. K. A nanostructured $SiAl_{0.2}O$ anode material for lithium batteries. *Chem. Mater.* **2010**, *22*, 5570–5579.
[115] Kim, K.; Choi, H.; Kim, J. H. Effect of carbon coating on nano-Si embedded SiO_x-Al_2O_3 composites as lithium storage materials. *Appl. Surf. Sci.* **2017**, *416*, 527–535.
[116] Lotfabad, E. M.; Kalisvaart, P.; Kohandehghan, A.; Cui, K.; Kupsta, M.; Farbod, B.; Mitlin, D. Si nanotubes ALD coated with TiO_2, TiN or Al_2O_3 as high performance lithium ion battery anodes. *J. Mater. Chem. A* **2014**, *2*, 2504–2516.
[117] Song, Y. H.; Zuo, L.; Chen, S. H.; Wu, J. F.; Hou, H. Q.; Wang, L. Porous nano-Si/carbon derived from zeolitic imidazolate frameworks@nano-Si as anode materials for lithium-ion batteries. *Electrochim. Acta* **2015**, *173*, 588–594.
[118] Jeong, G.; Kim, J. H.; Kim, Y. U.; Kim, Y. J. Multifunctional TiO_2 coating for a SiO anode in Li-ion batteries. *J. Mater. Chem.* **2012**, *22*, 7999–8004.
[119] Wu, H.; Yu, G. H.; Pan, L. J.; Liu, N.; McDowell, M. T.; Bao, Z. N.; Cui, Y. Stable Li-ion battery anodes by *in-situ* polymerization of conducting hydrogel to conformally coat silicon nanoparticles. *Nat. Commun.* **2013**, *4*, 1943.
[120] Park, S. J.; Zhao, H.; Ai, G.; Wang, C.; Song, X. Y.; Yuca, N.; Battaglia, V. S.; Yang, W. L.; Liu, G. Side-chain conducting and phase-separated polymeric binders for high-performance silicon anodes in lithium-ion batteries. *J. Am. Chem. Soc.* **2015**, *137*, 2565–2571.
[121] Higgins, T. M.; Park, S. H.; King, P. J.; Zhang, C. F.; McEvoy, N.; Berner, N. C.; Daly, D.; Shmeliov, A.; Khan, U.; Duesberg, G. et al. A commercial conducting polymer as both binder and conductive additive for silicon nanoparticle-based lithium-ion battery negative electrodes. *ACS Nano* **2016**, *10*, 3702–3713.
[122] Wang, Q. Y.; Zhu, M.; Chen, G. R.; Dudko, N.; Li, Y.; Liu, H. J.; Shi, L. Y.; Wu, G.; Zhang, D. S. High-performance microsized Si anodes for lithium-ion batteries: Insights into the polymer configuration conversion mechanism. *Adv. Mater.* **2022**, *34*, 2109658.
[123] Guo, J. P.; Zhao, G. M.; Xie, T.; Dong, D. Q.; Ma, C. L.; Su, L. H.; Gong, L. Y.; Lou, X. D.; Guo, X. Y.; Wang, J. et al. Carbon/polymer bilayer-coated Si-SiO_x electrodes with enhanced electrical conductivity and structural stability. *ACS Appl. Mater. Interfaces* **2020**, *12*, 19023–19032.
[124] Jiang, S. S.; Hu, B.; Sahore, R.; Zhang, L. H.; Liu, H. H.; Zhang, L.; Lu, W. Q.; Zhao, B.; Zhang, Z. C. Surface-functionalized silicon nanoparticles as anode material for lithium-ion battery. *ACS Appl. Mater. Interfaces* **2018**, *10*, 44924–44931.
[125] Li, C.; Shi, T. F.; Li, D. C.; Yoshitake, H.; Wang, H. Y. Effect of surface modification on electrochemical performance of nano-sized Si as an anode material for Li-ion batteries. *RSC Adv.* **2016**, *6*, 34715–34723.
[126] Zhao, J.; Lu, Z. D.; Wang, H. T.; Liu, W.; Lee, H. W.; Yan, K.; Zhuo, D.; Lin, D. C.; Liu, N.; Cui, Y. Artificial solid electrolyte interphase-protected Li_xSi nanoparticles: An efficient and stable prelithiation reagent for lithium-ion batteries. *J. Am. Chem. Soc.* **2015**, *137*, 8372–8375.
[127] Guo, J. P.; Wu, W.; Wang, J.; Zhang, T.; Wang, R.; Xu, D. W.; Wang, C. Y.; Deng, Y. H. Artificial solid electrolyte interphase modified porous SiO_x composite as anode material for lithium ion batteries. *Solid State Ionics* **2020**, *347*, 115272.
[128] Li, J. T.; Wu, Z. Y.; Lu, Y. Q.; Zhou, Y.; Huang, Q. S.; Huang, L.; Sun, S. G. Water soluble binder, an electrochemical performance booster for electrode materials with high energy density. *Adv. Energy Mater.* **2017**, *7*, 1701185.
[129] Chou, S. L.; Pan, Y. D.; Wang, J. Z.; Liu, H. K.; Dou, S. X. Small things make a big difference: Binder effects on the performance of Li and Na batteries. *Phys. Chem. Chem. Phys.* **2014**, *16*, 20347–20359.
[130] Hochgatterer, N. S.; Schweiger, M. R.; Koller, S.; Raimann, P. R.; Wöhrle, T.; Wurm, C.; Winter, M. Silicon/graphite composite electrodes for high-capacity anodes: Influence of binder chemistry on cycling stability. *Electrochem. Solid-State Lett.* **2008**, *11*, A76–A80.
[131] Chen, H.; Ling, M.; Hencz, L.; Ling, H. Y.; Li, G. R.; Lin, Z.; Liu, G.; Zhang, S. Q. Exploring chemical, mechanical, and electrical functionalities of binders for advanced energy-storage devices. *Chem. Rev.* **2018**, *118*, 8936–8982.
[132] Chen, L. B.; Xie, X. H.; Xie, J. Y.; Wang, K.; Yang, J. Binder effect on cycling performance of silicon/carbon composite anodes for lithium ion batteries. *J. Appl. Electrochem.* **2006**, *36*, 1099–1104.
[133] Wang, C.; Wu, H.; Chen, Z.; McDowell, M. T.; Cui, Y.; Bao, Z. N. Self-healing chemistry enables the stable operation of silicon microparticle anodes for high-energy lithium-ion batteries. *Nat. Chem.* **2013**, *5*, 1042–1048.
[134] Lopez, J.; Chen, Z.; Wang, C.; Andrews, S. C.; Cui, Y.; Bao, Z. N. The effects of cross-linking in a supramolecular binder on cycle life in silicon microparticle anodes. *ACS Appl. Mater. Interfaces* **2016**, *8*, 2318–2324.
[135] Munaoka, T.; Yan, X. Z.; Lopez, J.; To, J. W. F.; Park, J.; Tok, J. B. H.; Cui, Y.; Bao, Z. N. Ionically conductive self-healing binder for low cost Si microparticles anodes in Li-ion batteries. *Adv. Energy Mater.* **2018**, *8*, 1703138.
[136] Gordon, R.; Orias, R.; Willenbacher, N. Effect of carboxymethyl cellulose on the flow behavior of lithium-ion battery anode slurries and the electrical as well as mechanical properties of corresponding dry layers. *J. Mater. Sci.* **2020**, *55*, 15867–15881.
[137] Hu, B.; Jiang, S. S.; Shkrob, I. A.; Zhang, J. J.; Trask, S. E.; Polzin, B. J.; Jansen, A.; Chen, W.; Liao, C.; Zhang, Z. C. et al. Understanding of pre-lithiation of poly(acrylic acid) binder: Striking the balances between the cycling performance and slurry stability for silicon-graphite composite electrodes in Li-ion batteries. *J. Power Sources* **2019**, *416*, 125–131.
[138] Li, J.; Lewis, R. B.; Dahn, J. R. Sodium carboxymethyl cellulose: A potential binder for Si negative electrodes for Li-ion batteries. *Electrochem. Solid-State Lett.* **2007**, *10*, A17–A20.
[139] Kovalenko, I.; Zdyrko, B.; Magasinski, A.; Hertzberg, B.; Milicev, Z.; Burtovyy, R.; Luzinov, I.; Yushin, G. A major constituent of brown algae for use in high-capacity Li-ion batteries. *Science* **2011**, *334*, 75–79.

[140] Yue, L.; Zhang, L. Z.; Zhong, H. X. Carboxymethyl chitosan: A new water soluble binder for Si anode of Li-ion batteries. *J. Power Sources* **2014**, *247*, 327–331.
[141] Komaba, S.; Shimomura, K.; Yabuuchi, N.; Ozeki, T.; Yui, H.; Konno, K. Study on polymer binders for high-capacity SiO negative electrode of Li-ion batteries. *J. Phys. Chem. C* **2011**, *115*, 13487–13495.
[142] Aoki, S.; Han, Z. J.; Yamagiwa, K.; Yabuuchi, N.; Murase, M.; Okamoto, K.; Kiyosu, T.; Satoh, M.; Komaba, S. Acrylic acid-based copolymers as functional binder for silicon/graphite composite electrode in lithium-ion batteries. *J. Electrochem. Soc.* **2015**, *162*, A2245–A2249.
[143] Nguyen, C. C.; Seo, D. M.; Chandrasiri, K. W. D. K.; Lucht, B. L. Improved cycling performance of a Si nanoparticle anode utilizing citric acid as a surface-modifying agent. *Langmuir* **2017**, *33*, 9254–9261.
[144] Zhang, H.; Liu, S. W.; Yu, X. F.; Chen, S. L. Improving rate capacity and cycling stability of Si-anode lithium ion battery by using copper nanowire as conductive additive. *J. Alloys Compd.* **2020**, *822*, 153664.
[145] Wang, F.; Song, C. S.; Zhao, B. X.; Sun, L.; Du, H. B. One-pot solution synthesis of carbon-coated silicon nanoparticles as an anode material for lithium-ion batteries. *Chem. Commun.* **2020**, *56*, 1109–1112.
[146] Zhang, C. C.; Cai, X.; Chen, W. Y.; Yang, S. Y.; Xu, D. H.; Fang, Y. P.; Yu, X. Y. 3D porous silicon/N-doped carbon composite derived from bamboo charcoal as high-performance anode material for lithium-ion batteries. *ACS Sustainable Chem. Eng.* **2018**, *6*, 9930–9939.
[147] Ma, C. L.; Wang, Z. R.; Zhao, Y.; Li, Y.; Shi, J. A novel raspberry-like yolk–shell structured Si/C micro/nano-spheres as high-performance anode materials for lithium-ion batteries. *J. Alloys Compd.* **2020**, *844*, 156201.
[148] Jia, H. P.; Li, X. L.; Song, J. H.; Zhang, X.; Luo, L. L.; He, Y.; Li, B. S.; Cai, Y.; Hu, S. Y.; Xiao, X. C. et al. Hierarchical porous silicon structures with extraordinary mechanical strength as high-performance lithium-ion battery anodes. *Nat. Commun.* **2020**, *11*, 1474.
[149] Park, S. W.; Shim, H. W.; Kim, J. C.; Kim, D. W. Uniform Si nanoparticle-embedded nitrogen-doped carbon nanofiber electrodes for lithium ion batteries. *J. Alloys Compd.* **2017**, *728*, 490–496.
[150] Kim, S. J.; Moon, S. H.; Kim, M. C.; So, J. Y.; Han, S. B.; Kwak, D. H.; Bae, W. G.; Park, K. W. Micro-patterned 3D Si electrodes fabricated using an imprinting process for high-performance lithium-ion batteries. *J. Appl. Electrochem.* **2018**, *48*, 1057–1068.
[151] Wu, J. L.; Liu, J. H.; Wang, Z.; Gong, X. Z.; Wang, Y. A new design for Si wears double jackets used as a high-performance lithium-ion battery anode. *Chem. Eng. J.* **2019**, *370*, 565–572.
[152] Song, J. J.; Guo, S. W.; Kou, L. J.; Kajiyoshi, K.; Su, J. X.; Huang, W. R.; Li, Y. F.; Zheng, P. Controllable synthesis honeycomb-like structure SiO_x/C composites as anode for high-performance lithium-ion batteries. *Vacuum* **2021**, *186*, 110044.
[153] Mishra, K.; Zheng, J. M.; Patel, R.; Estevez, L.; Jia, H. P.; Luo, L. L.; El-Khoury, P. Z.; Li, X. L.; Zhou, X. D.; Zhang, J. G. High performance porous Si@C anodes synthesized by low temperature aluminothermic reaction. *Electrochim. Acta* **2018**, *269*, 509–516.
[154] Ma, B. J.; Lu, B.; Luo, J.; Deng, X. L.; Wu, Z. Y.; Wang, X. Y. The hollow mesoporous silicon nanobox dually encapsulated by SnO_2/C as anode material of lithium ion battery. *Electrochim. Acta* **2018**, *288*, 61–70.
[155] Tang, C. J.; Liu, Y. N.; Xu, C.; Zhu, J. X.; Wei, X. J.; Zhou, L.; He, L.; Yang, W.; Mai, L. Ultrafine nickel-nanoparticle-enabled SiO_2 hierarchical hollow spheres for high-performance lithium storage. *Adv. Funct. Mater.* **2018**, *28*, 1704561.
[156] Jia, H. P.; Zheng, J. M.; Song, J. H.; Luo, L. L.; Yi, R.; Estevez, L.; Zhao, W. G.; Patel, R.; Li, X. L.; Zhang, J. G. A novel approach to synthesize micrometer-sized porous silicon as a high performance anode for lithium-ion batteries. *Nano Energy* **2018**, *50*, 589–597.
[157] Yang, W. T.; Ying, H. J.; Zhang, S. L.; Guo, R. N.; Wang, J. L.; Han, W. Q. Electrochemical performance enhancement of porous Si lithium-ion battery anode by integrating with optimized carbonaceous materials. *Electrochim. Acta* **2020**, *337*, 135687.
[158] Yang, Y. H.; Liu, S.; Bian, X. F.; Feng, J. K.; An, Y. L.; Yuan, C. Morphology- and porosity-tunable synthesis of 3D nanoporous SiGe alloy as a high-performance lithium-ion battery anode. *ACS Nano* **2018**, *12*, 2900–2908.
[159] Xu, Q.; Li, J. Y.; Sun, J. K.; Yin, Y. X.; Wan, L. J.; Guo, Y. G. Watermelon-inspired Si/C microspheres with hierarchical buffer structures for densely compacted lithium-ion battery anodes. *Adv. Energy Mater.* **2017**, *7*, 1601481.
[160] Kim, D.; Li, N.; Sheehan, C. J.; Yoo, J. Degradation of Si/Ge core/shell nanowire heterostructures during lithiation and delithiation at 0.8 and 20 $A \cdot g^{-1}$. *Nanoscale* **2018**, *10*, 7343–7351.
[161] Stokes, K.; Boonen, W.; Geaney, H.; Kennedy, T.; Borsa, D.; Ryan, K. M. Tunable core–shell nanowire active material for high capacity Li-ion battery anodes comprised of PECVD deposited aSi on directly grown Ge nanowires. *ACS Appl. Mater. Interfaces* **2019**, *11*, 19372–19380.
[162] Yang, J. C.; Liu, J.; Zhao, C. N.; Zhang, W. Q.; Li, X. C. Core–shell structured heterohierachical porous Si@graphene microsphere for high-performance lithium-ion battery anodes. *Mater. Lett.* **2020**, *266*, 127484.
[163] Li, Z. L.; Zhao, H. L.; Lv, P. P.; Zhang, Z. J.; Zhang, Y.; Du, Z. H.; Teng, Y. Q.; Zhao, L. N.; Zhu, Z. M. Watermelon-like structured SiO_x-TiO_2@C nanocomposite as a high-performance lithium-ion battery anode. *Adv. Funct. Mater.* **2018**, *28*, 1605711.
[164] Li, B. B.; Jiang, Y. Z.; Jiang, F.; Cao, D. X.; Wang, H. K.; Niu, C. M. Bird's nest-like nanographene shell encapsulated Si nanoparticles—Their structural and Li anode properties. *J. Power Sources* **2017**, *341*, 46–52.
[165] Zhao, T. L.; Meng, Y.; Yin, H. S.; Guo, K. J.; Ji, R. X.; Zhang, G. L.; Zhang, Y. X. Beneficial effect of green water-soluble binders on SiO_x/graphite anode for lithium-ion batteries. *Chem. Phys. Lett.* **2020**, *742*, 137145.
[166] Wang, X. X.; Liu, J.; Gong, Z. L.; Huang, C. F.; He, S. S.; Yu, L. B.; Gan, L. H.; Long, M. N. Influence of degree of substitution of carboxymethyl cellulose on high performance silicon anode in lithium-ion batteries. *Electrochemistry* **2019**, *87*, 94–99.
[167] Kim, S.; Jeong, Y. K.; Wang, Y.; Lee, H.; Choi, J. W. A "sticky" mucin-inspired DNA-polysaccharide binder for silicon and silicon-graphite blended anodes in lithium-ion batteries. *Adv. Mater.* **2018**, *30*, e1707594.
[168] Magasinski, A.; Zdyrko, B.; Kovalenko, I.; Hertzberg, B.; Burtovyy, R.; Huebner, C. F.; Fuller, T. F.; Luzinov, I.; Yushin, G. Toward efficient binders for Li-ion battery Si-based anodes: Polyacrylic acid. *ACS Appl. Mater. Interfaces* **2010**, *2*, 3004–3010.
[169] Koo, B.; Kim, H.; Cho, Y.; Lee, K. T.; Choi, N. S.; Cho, J. A highly cross-linked polymeric binder for high-performance silicon negative electrodes in lithium ion batteries. *Angew. Chem., Int. Ed.* **2012**, *51*, 8762–8767.
[170] Hwang, C.; Joo, S.; Kang, N. R.; Lee, U.; Kim, T. H.; Jeon, Y.; Kim, J.; Kim, Y. J.; Kim, J. Y.; Kwak, S. K. et al. Breathing silicon anodes for durable high-power operations. *Sci. Rep.* **2015**, *5*, 14433.
[171] Yoon, D.-E.; Hwang, C.; Kang, N.-R.; Lee, U.; Ahn, D.; Kim, J.-Y.; Song, H.-K. Dependency of electrochemical performances of silicon lithium-ion batteries on glycosidic linkages of polysaccharide binders. *ACS Appl. Mater. Interfaces* **2016**, *8*, 4042–4047.
[172] Urbanski, A.; Omar, A.; Guo, J.; Janke, A.; Reuter, U.; Malanin, M.; Schmidt, F.; Jehnichen, D.; Holzschuh, M.; Simon, F. et al. An efficient two-polymer binder for high-performance silicon nanoparticle-based lithium-ion batteries: A systematic case study with commercial polyacrylic acid and polyvinyl butyral polymers. *J. Electrochem. Soc.* **2019**, *166*, A5275–A5286.
[173] Huang, Q. Y.; Wan, C. Y.; Loveridge, M.; Bhagat, R. Partially neutralized polyacrylic acid/poly(vinyl alcohol) blends as effective binders for high-performance silicon anodes in lithium-ion batteries. *ACS Appl. Energy Mater.* **2018**, *1*, 6890–6898.
[174] Song, J. X.; Zhou, M. J.; Yi, R.; Xu, T.; Gordin, M. L.; Tang, D. H.; Yu, Z. X.; Regula, M.; Wang, D. H. Interpenetrated gel

polymer binder for high-performance silicon anodes in lithium-ion batteries. *Adv. Funct. Mater.* **2014**, *24*, 5904–5910.

[175] Wang, X. Y.; Zhang, Y.; Shi, Y. J.; Zeng, X. Y.; Tang, R. X.; Wei, L. M. Conducting polyaniline/poly (acrylic acid)/phytic acid multifunctional binders for Si anodes in lithium ion batteries. *Ionics* **2019**, *25*, 5323–5331.

[176] Li, Z. H.; Zhang, Y. P.; Liu, T. F.; Gao, X. H.; Li, S. Y.; Ling, M.; Liang, C. D.; Zheng, J. C.; Lin, Z. Silicon anode with high initial coulombic efficiency by modulated trifunctional binder for high-areal-capacity lithium-ion batteries. *Adv. Energy Mater.* **2020**, *10*, 1903110.

[177] Li, J. J.; Zhang, G. Z.; Yang, Y.; Yao, D. H.; Lei, Z. W.; Li, S.; Deng, Y. H.; Wang, C. Y. Glycinamide modified polyacrylic acid as high-performance binder for silicon anodes in lithium-ion batteries. *J. Power Sources* **2018**, *406*, 102–109.

[178] Wang, J. T.; Wan, C. C.; Hong, J. L. Polymer blends of pectin/poly(acrylic acid) as efficient binders for silicon anodes in lithium-ion batteries. *ChemElectroChem* **2020**, *7*, 3106–3115.

[179] Cao, P. F.; Naguib, M.; Du, Z. J.; Stacy, E.; Li, B. R.; Hong, T.; Xing, K. Y.; Voylov, D. N.; Li, J. L.; Wood, D. L. et al. Effect of binder architecture on the performance of silicon/graphite composite anodes for lithium ion batteries. *ACS Appl. Mater. Interfaces* **2018**, *10*, 3470–3478.

[180] Gao, Y.; Qiu, X. T.; Wang, X. L.; Gu, A. Q.; Zhang, L.; Chen, X. C.; Li, J. F.; Yu, Z. L. Chitosan-g-poly(acrylic acid) copolymer and its sodium salt as stabilized aqueous binders for silicon anodes in lithium-ion batteries. *ACS Sustainable Chem. Eng.* **2019**, *7*, 16274–16283.

[181] Cao, P. F.; Yang, G.; Li, B. R.; Zhang, Y. M.; Zhao, S.; Zhang, S.; Erwin, A.; Zhang, Z. C.; Sokolov, A. P.; Nanda, J. et al. Rational design of a multifunctional binder for high-capacity silicon-based anodes. *ACS Energy Lett.* **2019**, *4*, 1171–1180.

[182] Feng, K.; Li, M.; Zhang, Y. N.; Liu, W. W.; Kashkooli, A. G.; Xiao, X. C.; Chen, Z. W. Micron-sized secondary Si/C composite with *in situ* crosslinked polymeric binder for high-energy-density lithium-ion battery anode. *Electrochim. Acta* **2019**, *309*, 157–165.

[183] Guo, R. N.; Zhang, S. L.; Ying, H. J.; Yang, W. T.; Wang, J. L.; Han, W. Q. Preparation of an amorphous cross-linked binder for silicon anodes. *ChemSusChem* **2019**, *12*, 4838–4845.

[184] He, D. L.; Li, P.; Wang, W.; Wan, Q.; Zhang, J.; Xi, K.; Ma, X. M.; Liu, Z. W.; Zhang, L.; Qu, X. H. Collaborative design of hollow nanocubes, *in situ* cross-linked binder, and amorphous void@SiO_x@C as a three-pronged strategy for ultrastable lithium storage. *Small* **2020**, *16*, e1905736.

[185] Jeschull, F.; Scott, F.; Trabesinger, S. Interactions of silicon nanoparticles with carboxymethyl cellulose and carboxylic acids in negative electrodes of lithium-ion batteries. *J. Power Sources* **2019**, *431*, 63–74.

[186] Son, J.; Vo, T. N.; Cho, S.; Preman, A. N.; Kim, I. T.; Ahn, S. K. Acrylic random copolymer and network binders for silicon anodes in lithium-ion batteries. *J. Power Sources* **2020**, *458*, 228054.

[187] Tian, M.; Wu, P. Y. Nature plant polyphenol coating silicon submicroparticle conjugated with polyacrylic acid for achieving a high-performance anode of lithium-ion battery. *ACS Appl. Energy Mater.* **2019**, *2*, 5066–5073.

[188] Zhu, X. Y.; Zhang, F.; Zhang, L.; Zhang, L. Y.; Song, Y. Z.; Jiang, T.; Sayed, S.; Lu, C.; Wang, X. G.; Sun, J. Y. et al. A highly stretchable cross-linked polyacrylamide hydrogel as an effective binder for silicon and sulfur electrodes toward durable lithium-ion storage. *Adv. Funct. Mater.* **2018**, *28*, 1705015.

[189] Cai, Y. J.; Li, Y. Y.; Jin, B. Y.; Ali, A.; Ling, M.; Cheng, D. G.; Lu, J. G.; Hou, Y.; He, Q. G.; Zhan, X. L. et al. Dual cross-linked fluorinated binder network for high-performance silicon and silicon oxide based anodes in lithium-ion batteries. *ACS Appl. Mater. Interfaces* **2019**, *11*, 46800–46807.

[190] Chen, C.; Chen, F.; Liu, L. M.; Zhao, J. W.; Wang, F. Cross-linked hyperbranched polyethylenimine as an efficient multidimensional binder for silicon anodes in lithium-ion batteries. *Electrochim. Acta* **2019**, *326*, 134964.

[191] Zhu, L. L.; Du, F. H.; Zhuang, Y.; Dai, H.; Cao, H. S.; Adkins, J.; Zhou, Q.; Zheng, J. W. Effect of crosslinking binders on Li-storage behavior of silicon particles as anodes for lithium ion batteries. *J. Electroanal. Chem.* **2019**, *845*, 22–30.

[192] Liu, N.; He, W. J.; Liao, H. J.; Li, Z. W.; Jiang, J. M.; Zhang, X. G.; Dou, H. Polydopamine grafted cross-linked polyacrylamide as robust binder for SiO/C anode toward high-stability lithium-ion battery. *J. Mater. Sci.* **2021**, *56*, 6337–6348.

[193] Assresahegn, B. D.; Bélanger, D. Synthesis of binder-like molecules covalently linked to silicon nanoparticles and application as anode material for lithium-ion batteries without the use of electrolyte additives. *J. Power Sources* **2017**, *345*, 190–201.

[194] Chae, S.; Kwak, W. J.; Han, K. S.; Li, S.; Engelhard, M. H.; Hu, J. T.; Wang, C. M.; Li, X. L.; Zhang, J. G. Rational design of electrolytes for long-term cycling of Si anodes over a wide temperature range. *ACS Energy Lett.* **2021**, *6*, 387–394.

[195] Guo, J.; Omar, A.; Urbanski, A.; Oswald, S.; Uhlmann, P.; Giebeler, L. Electrochemical behavior of microparticulate silicon anodes in ether-based electrolytes: Why does $LiNO_3$ affect negatively? *ACS Appl. Energy Mater.* **2019**, *2*, 4411–4420.

[196] Han, B. H.; Liao, C.; Dogan, F.; Trask, S. E.; Lapidus, S. H.; Vaughey, J. T.; Key, B. Using mixed salt electrolytes to stabilize silicon anodes for lithium-ion batteries via *in situ* formation of Li-M-Si ternaries (M = Mg, Zn, Al, Ca). *ACS Appl. Mater. Interfaces* **2019**, *11*, 29780–29790.

[197] Huang, F. F.; Ma, G. Q.; Wen, Z. Y.; Jin, J.; Xu, S. Q.; Zhang, J. J. Enhancing metallic lithium battery performance by tuning the electrolyte solution structure. *J. Mater. Chem. A* **2018**, *6*, 1612–1620.

[198] Jia, H. P.; Zou, L. F.; Gao, P. Y.; Cao, X.; Zhao, W. G.; He, Y.; Engelhard, M. H.; Burton, S. D.; Wang, H.; Ren, X. D. et al. High-performance silicon anodes enabled by nonflammable localized high-concentration electrolytes. *Adv. Energy Mater.* **2019**, *9*, 1900784.

[199] Louli, A. J.; Ellis, L. D.; Dahn, J. R. Operando pressure measurements reveal solid electrolyte interphase growth to rank Li-ion cell performance. *Joule* **2019**, *3*, 745–761.

[200] Luo, W.; Chen, X. Q.; Xia, Y.; Chen, M.; Wang, L. J.; Wang, Q. Q.; Li, W.; Yang, J. P. Surface and interface engineering of silicon-based anode materials for lithium-ion batteries. *Adv. Energy Mater.* **2017**, *7*, 1701083.

[201] Markevich, E.; Salitra, G.; Aurbach, D. Fluoroethylene carbonate as an important component for the formation of an effective solid electrolyte interphase on anodes and cathodes for advanced Li-ion batteries. *ACS Energy Lett.* **2017**, *2*, 1337–1345.

[202] Michan, A. L.; Divitini, G.; Pell, A. J.; Leskes, M.; Ducati, C.; Grey, C. P. Solid electrolyte interphase growth and capacity loss in silicon electrodes. *J. Am. Chem. Soc.* **2016**, *138*, 7918–7931.

[203] Peng, Z.; Cao, X.; Gao, P. Y.; Jia, H. P.; Ren, X. D.; Roy, S.; Li, Z. D.; Zhu, Y.; Xie, W. P.; Liu, D. Y. et al. High-power lithium metal batteries enabled by high-concentration acetonitrile-based electrolytes with vinylene carbonate additive. *Adv. Funct. Mater.* **2020**, *30*, 2001285.

[204] Haregewoin, A. M.; Wotango, A. S.; Hwang, B. J. Electrolyte additives for lithium ion battery electrodes: Progress and perspectives. *Energy Environ. Sci.* **2016**, *9*, 1955–1988.

[205] Gebresilassie Eshetu, G.; Martinez-Ibañez, M.; Sánchez-Diez, E.; Gracia, I.; Li, C. M.; Rodriguez-Martinez, L. M.; Rojo, T.; Zhang, H.; Armand, M. Electrolyte additives for room-temperature, sodium-based, rechargeable batteries. *Chem.—Asian J.* **2018**, *13*, 2770–2780.

[206] Choi, N. S.; Yew, K. H.; Lee, K. Y.; Sung, M.; Kim, H.; Kim, S. S. Effect of fluoroethylene carbonate additive on interfacial properties of silicon thin-film electrode. *J. Power Sources* **2006**, *161*, 1254–1259.

[207] Jin, Y. T.; Kneusels, N. J. H.; Magusin, P. C. M. M.; Kim, G.; Castillo-Martínez, E.; Marbella, L. E.; Kerber, R. N.; Howe, D. J.; Paul, S.; Liu, T. et al. Identifying the structural basis for the increased stability of the solid electrolyte interphase formed on silicon with the additive fluoroethylene carbonate. *J. Am. Chem. Soc.* **2017**, *139*, 14992–15004.

[208] Jung, R.; Metzger, M.; Haering, D.; Solchenbach, S.; Marino, C.; Tsiouvaras, N.; Stinner, C.; Gasteiger, H. A. Consumption of

fluoroethylene carbonate (FEC) on Si-C composite electrodes for Li-ion batteries. *J. Electrochem. Soc.* **2016**, *163*, A1705–A1716.
[209] Zhou, M.; Jin, C.; Zheng, W.; Liang, Y. R.; Shi, Q.; Yuan, Y. N.; Zheng, H. H. A novel MEMP-DFOB electrolyte additive to improve low-high temperature performances of SiO/Gr anode based pouch full cells. *J. Electroanal. Chem.* **2021**, *898*, 115639.
[210] Matsumoto, K.; Inoue, K.; Utsugi, K. A highly safe battery with a non-flammable triethyl-phosphate-based electrolyte. *J. Power Sources* **2015**, *273*, 954–958.
[211] Cao, Z.; Zheng, X. T.; Qu, Q. T.; Huang, Y. H.; Zheng, H. H. Electrolyte design enabling a high-safety and high-performance Si anode with a tailored electrode-electrolyte interphase. *Adv. Mater.* **2021**, *33*, 2103178.
[212] Lewandowski, A.; Świderska-Mocek, A. Ionic liquids as electrolytes for Li-ion batteries-an overview of electrochemical studies. *J. Power Sources* **2009**, *194*, 601–609.
[213] Molina Piper, D.; Evans, T.; Leung, K.; Watkins, T.; Olson, J.; Kim, S. C.; Han, S. S.; Bhat, V.; Oh, K. H.; Buttry, D. A. et al. Stable silicon-ionic liquid interface for next-generation lithium-ion batteries. *Nat. Commun.* **2015**, *6*, 6230.
[214] Song, J. W.; Nguyen, C. C.; Song, S. W. Stabilized cycling performance of silicon oxide anode in ionic liquid electrolyte for rechargeable lithium batteries. *RSC Adv.* **2012**, *2*, 2003–2009.
[215] Guo, S. T.; Li, H.; Li, Y. Q.; Han, Y.; Chen, K. B.; Xu, G. Z.; Zhu, Y. J.; Hu, X. L. SiO_2-enhanced structural stability and strong adhesion with a new binder of konjac glucomannan enables stable cycling of silicon anodes for lithium-ion batteries. *Adv. Energy Mater.* **2018**, *8*, 1800434.
[216] Bie, Y. T.; Yang, J.; Liu, X. L.; Wang, J. L.; Nuli, Y.; Lu, W. Polydopamine wrapping silicon cross-linked with polyacrylic acid as high-performance anode for lithium-ion batteries. *ACS Appl. Mater. Interfaces* **2016**, *8*, 2899–2904.
[217] Miranda, A.; Li, X. Y.; Haregewoin, A. M.; Sarang, K.; Lutkenhaus, J.; Kostecki, R.; Verduzco, R. A comprehensive study of hydrolyzed polyacrylamide as a binder for silicon anodes. *ACS Appl. Mater. Interfaces* **2019**, *11*, 44090–44100.
[218] He, J. R.; Zhang, L. Z. Polyvinyl alcohol grafted poly(acrylic acid) as water-soluble binder with enhanced adhesion capability and electrochemical performances for Si anode. *J. Alloys Compd.* **2018**, *763*, 228–240.
[219] Jung, C. H.; Kim, K. H.; Hong, S. H. Stable silicon anode for lithium-ion batteries through covalent bond formation with a binder via esterification. *ACS Appl. Mater. Interfaces* **2019**, *11*, 26753–26763.
[220] Parikh, P.; Sina, M.; Banerjee, A.; Wang, X. F.; D'Souza, M. S.; Doux, J. M.; Wu, E. A.; Trieu, O. Y.; Gong, Y. B.; Zhou, Q. et al. Role of polyacrylic acid (PAA) binder on the solid electrolyte interphase in silicon anodes. *Chem. Mater.* **2019**, *31*, 2535–2544.
[221] Yao, D. H.; Yang, Y.; Deng, Y. H.; Wang, C. Y. Flexible polyimides through one-pot synthesis as water-soluble binders for silicon anodes in lithium ion batteries. *J. Power Sources* **2018**, *379*, 26–32.
[222] Yao, D. H.; Feng, J. W.; Wang, J.; Deng, Y. H.; Wang, C. Y. Synthesis of silicon anode binders with ultra-high content of catechol groups and the effect of molecular weight on battery performance. *J. Power Sources* **2020**, *463*, 228188.
[223] Rajeev, K. K.; Kim, E.; Nam, J.; Lee, S.; Mun, J.; Kim, T. H. Chitosan-grafted-polyaniline copolymer as an electrically conductive and mechanically stable binder for high-performance Si anodes in Li-ion batteries. *Electrochim. Acta* **2020**, *333*, 135532.
[224] Kim, E.; K, K. R.; Nam, J.; Mun, J.; Kim, T. H. Chitosan-grafted-poly(aniline-co-anthranilic acid) as a water soluble binder to form 3D structures for Si anodes. *RSC Adv.* **2020**, *10*, 7643–7653.
[225] Kuo, T. C.; Chiou, C. Y.; Li, C. C.; Lee, J. T. *In situ* cross-linked poly(ether urethane) elastomer as a binder for high-performance Si anodes of lithium-ion batteries. *Electrochim. Acta* **2019**, *327*, 135011.
[226] Liu, X. J.; Zai, J. T.; Iqbal, A.; Chen, M.; Ali, N.; Qi, R. R.; Qian, X. F. Glycerol-crosslinked PEDOT: PSS as bifunctional binder for Si anodes: Improved interfacial compatibility and conductivity. *J. Colloid Interface Sci.* **2020**, *565*, 270–277.
[227] Liu, X. J.; Iqbal, A.; Ali, N.; Qi, R. R.; Qian, X. F. Ion-cross-linking-promoted high-performance Si/PEDOT: PSS electrodes: The importance of cations' ionic potential and softness parameters. *ACS Appl. Mater. Interfaces* **2020**, *12*, 19431–19438.
[228] Liu, D.; Zhao, Y.; Tan, R.; Tian, L. L.; Liu, Y. D.; Chen, H. B.; Pan, F. Novel conductive binder for high-performance silicon anodes in lithium ion batteries. *Nano Energy* **2017**, *36*, 206–212.
[229] Zhang, J. H.; Wang, N.; Zhang, W.; Fang, S.; Yu, Z. L.; Shi, B. M.; Yang, J. Y. A cycling robust network binder for high performance Si-based negative electrodes for lithium-ion batteries. *J. Colloid Interface Sci.* **2020**, *578*, 452–460.
[230] Zhao, H.; Wei, Y.; Qiao, R. M.; Zhu, C. H.; Zheng, Z. Y.; Ling, M.; Jia, Z.; Bai, Y.; Fu, Y. B.; Lei, J. L. et al. Conductive polymer binder for high-tap-density nanosilicon material for lithium-ion battery negative electrode application. *Nano Lett.* **2015**, *15*, 7927–7932.
[231] Choi, S.; Kwon, T. W.; Coskun, A.; Choi, J. W. Highly elastic binders integrating polyrotaxanes for silicon microparticle anodes in lithium ion batteries. *Science* **2017**, *357*, 279–283.
[232] Dufficy, M. K.; Khan, S. A.; Fedkiw, P. S. Galactomannan binding agents for silicon anodes in Li-ion batteries. *J. Mater. Chem. A* **2015**, *3*, 12023–12030.
[233] Lee, D.; Park, H.; Goliaszewski, A.; Byeun, Y. K.; Song, T.; Paik, U. *In situ* cross-linked carboxymethyl cellulose-polyethylene glycol binder for improving the long-term cycle life of silicon anodes in Li ion batteries. *Ind. Eng. Chem. Res.* **2019**, *58*, 8123–8130.
[234] Ryu, J.; Kim, S.; Kim, J.; Park, S.; Lee, S.; Yoo, S.; Kim, J.; Choi, N. S.; Ryu, J. H.; Park, S. Room-temperature crosslinkable natural polymer binder for high-rate and stable silicon anodes. *Adv. Funct. Mater.* **2020**, *30*, 1908433.
[235] Lim, S.; Lee, K.; Shin, I.; Tron, A.; Mun, J.; Yim, T.; Kim, T. H. Physically cross-linked polymer binder based on poly(acrylic acid) and ion-conducting poly(ethylene glycol-co-benzimidazole) for silicon anodes. *J. Power Sources* **2017**, *360*, 585–592.
[236] Yuca, N.; Cetintasoglu, M. E.; Dogdu, M. F.; Akbulut, H.; Tabanli, S.; Colak, U.; Taskin, O. S. Highly efficient poly(fluorene phenylene) copolymer as a new class of binder for high-capacity silicon anode in lithium-ion batteries. *Int. J. Energy Res.* **2018**, *42*, 1148–1157.
[237] Zhao, H.; Wei, Y.; Wang, C.; Qiao, R. M.; Yang, W. L.; Messersmith, P. B.; Liu, G. Mussel-inspired conductive polymer binder for Si-alloy anode in lithium-ion batteries. *ACS Appl. Mater. Interfaces* **2018**, *10*, 5440–5446.
[238] Wang, L.; Liu, T. F.; Peng, X.; Zeng, W. W.; Jin, Z. Z.; Tian, W. F.; Gao, B.; Zhou, Y. H.; Chu, P. K.; Huo, K. F. Highly stretchable conductive glue for high-performance silicon anodes in advanced lithium-ion batteries. *Adv. Funct. Mater.* **2018**, *28*, 1704858.
[239] Sun, L.; Liu, Y. X.; Shao, R.; Wu, J.; Jiang, R. Y.; Jin, Z. Recent progress and future perspective on practical silicon anode-based lithium ion batteries. *Energy Storage Mater.* **2022**, *46*, 482–502.
[240] Huang, Q. Q.; Song, J. X.; Gao, Y.; Wang, D. W.; Liu, S.; Peng, S. F.; Usher, C.; Goliaszewski, A.; Wang, D. H. Supremely elastic gel polymer electrolyte enables a reliable electrode structure for silicon-based anodes. *Nat. Commun.* **2019**, *10*, 5586.
[241] Cervera, R. B.; Suzuki, N.; Ohnishi, T.; Osada, M.; Mitsuishi, K.; Kambara, T.; Takada, K. High performance silicon-based anodes in solid-state lithium batteries. *Energy Environ. Sci.* **2014**, *7*, 662–666.
[242] Pan, J.; Peng, H. L.; Yan, Y. H.; Bai, Y. Z.; Yang, J.; Wang, N. N.; Dou, S. X.; Huang, F. Q. Solid-state batteries designed with high ion conductive composite polymer electrolyte and silicon anode. *Energy Storage Mater.* **2021**, *43*, 165–171.
[243] Pandey, G. P.; Klankowski, S. A.; Li, Y. H.; Sun, X. S.; Wu, J.; Rojeski, R. A.; Li, J. Effective infiltration of gel polymer electrolyte into silicon-coated vertically aligned carbon nanofibers as anodes for solid-state lithium-ion batteries. *ACS Appl. Mater. Interfaces* **2015**, *7*, 20909–20918.
[244] Poetke, S.; Hippauf, F.; Baasner, A.; Dörfler, S.; Althues, H.; Kaskel, S. Nanostructured Si-C composites as high-capacity anode material for all-solid-state lithium-ion batteries. *Batter. Supercaps*

2021, *4*, 1323–1334.
[245] Okuno, R.; Yamamoto, M.; Kato, A.; Takahashi, M. Microscopic observation of nanoporous Si-Li_3PS_4 interface in composite anodes with stable cyclability. *Electrochem. Commun.* **2021**, *130*, 107100.
[246] Kim, J.; Kim, C.; Jang, I.; Park, J.; Kim, J.; Paik, U.; Song, T. Si nanoparticles embedded in carbon nanofiber sheathed with Li_6PS_5Cl as an anode material for all-solid-state batteries. *J. Power Sources* **2021**, *510*, 230425.
[247] Meng, X. Y.; Liu, Y. Z.; Wang, Z. Z.; Zhang, Y. Z.; Wang, X. Y.; Qiu, J. S. A quasi-solid-state rechargeable cell with high energy and superior safety enabled by stable redox chemistry of Li_2S in gel electrolyte. *Energy Environ. Sci.* **2021**, *14*, 2278–2290.
[248] Shi, J. W.; Gao, H. Y.; Hu, G. X.; Zhang, Q. Interfacial self-assembled Si@SiO_x@C microclusters with high tap density for high-performance Li-ion batteries. *Mater. Today Energy* **2022**, *29*, 101090.
[249] Ge, M. Z.; Cao, C. Y.; Biesold, G. M.; Sewell, C. D.; Hao, S. M.; Huang, J. Y.; Zhang, W.; Lai, Y. K.; Lin, Z. Q. Recent advances in silicon-based electrodes: From fundamental research toward practical applications. *Adv. Mater.* **2021**, *33*, e2004577.